

國立交通大學

電信工程學系

碩士論文

寬頻手機天線之微小化設計

The logo of National Tsing Hua University is a circular emblem with a gear-like border. Inside the circle, there is a stylized building and the year '1896'.

**Miniaturization of Broadband Antennas for
Mobile handsets**

研究生：林育正

指導教授：唐震寰 教授

中華民國九十六年六月

寬頻手機天線之微小化設計

Miniaturization of Broadband Antennas for Mobile Handsets

研究生：林育正

Student：Yu-Cheng Lin

指導教授：唐震寰 教授

Advisor：Jenn-Hwan Tarn

國立交通大學

電信工程學系碩士班

碩士論文

A Thesis

Submitted to Department of Communication Engineering
College of Electrical Engineering and Computer Science

National Chiao Tung University

in Partial Fulfillment of the Requirements

for the Degree of

Master

in

Communication Engineering

June 2007

Hsinchu, Taiwan, Republic of China

中華民國九十六年六月

寬頻手機天線之微小化設計

研究生：林育正

指導教授：唐震寰 教授

國立交通大學

電信工程學系 碩士班

摘要

目前天線設計以滿足小尺寸與多頻帶兩大要求為主。多頻帶、小尺寸、天線場型及增益都是設計天線時重要的考量因子。然而這些因子彼此之間可能會相互衝突，所以設計時必須適當的折衝與取捨。本篇論文提出一個具有寬頻與小尺寸特性的天線，可以適用於 GPS，GSM 1800，PCS，3G，WLAN，與 WiMAX 等系統應用。該天線應用二項式曲線結構，能夠輕易滿足寬頻特性，並可藉由改變天線幾何形狀增加共振長度，達到微小化的目的。經由模擬與量測結果之比較，該天線的操作頻帶涵蓋 1.54 GHz 到 2.73 GHz，頻寬為 1.19 GHz。天線的體積為 $25 \times 25 \times 0.8(500) \text{ mm}^3$ ，小於文獻中其它天線設計的體積： 600 mm^3 ， 1135 mm^3 ， 1181 mm^3 或 1598 mm^3 。除此之外，這個天線具有近似單指向的 (Omni-directional) 輻射場型，且具有合理之增益，量測最大值介於 2.25 dBi-3.74 dBi 之間。

Miniaturization of Broadband Antennas for Mobile Handsets

Student : Yu-Cheng Lin

Advisor : Dr. Jenn-Hwan Tarnq

Department of Communication Engineering
National Chiao Tung University

Abstract

In nowadays, antenna design mainly focuses on size reduction and multi-band or broadband. However, in the design, multi-band, size reduction, radiation pattern, and antenna gain are the major issues to be considered. It is well-known that these issues are trade-offs one another. In the thesis, a broadband small antenna has been proposed for GPS, GSM 1800, PCS, 3G, WLAN, and WiMAX systems. By applying binomial curve structure, the proposed antenna can easily achieve a broad bandwidth. The miniaturization is achieved due to an increasing resonant length by properly adjusting geometrical parameters of the antenna. The simulated and measured results confirmed that the proposed antenna can operate at 1.54 GHz to 2.73 GHz bands with bandwidth of 1.19 GHz. The antenna occupies a compact volume of $25 \times 25 \times 0.8 \text{ mm}^3$, which is smaller than other designs of the volumes: 600 mm^3 , 1135 mm^3 , 1181 mm^3 or 1598 mm^3 . Moreover, the antenna has a nearly omni-directional radiation pattern and a reasonable peak gain of 2.25 dBi to 3.74 dBi.

誌 謝

在碩士研究的這二年歲月，首先要感謝的是我的指導教授 唐震寰教授並致上我最誠摯的謝意。感謝老師在專業的通訊領域中，給予我不斷的指導與鼓勵，並賦予了實驗室豐富的研究資源與環境，使得這篇碩士論文能夠順利完成。

其次，要感謝波散射與傳播實驗室的學長們—鄭世杰學長、劉文舜學長、莊博學長、宜興學長、和穆學長、孟勳學長、舜升學長、懷文學長在研究上的幫助與意見，讓我獲益良多。感謝實驗室的同學—奕慶、豐吉、志璋、思云、蓓鎮等在課業及研究上的互相砥礪與切磋，以及生活上的多彩多姿。感謝學弟們，讓實驗室在嚴肅的研究氣氛中增添了許多歡樂，有了你們，更加豐富了我這二年的研究生生活。感謝陳思穎小姐，協助我利用台大圖書館的資源，讓我突破每一次研究的瓶頸。另外，也要感謝助理—梁麗君小姐，在生活上的協助和籌劃每次的美食聚餐饗宴。

最後，要感謝的就是我最親愛的家人，由於他們在我求學過程中，一路陪伴著我，給予我最溫馨的關懷與鼓勵，讓我在人生的過程裡得到快樂，更讓我可以專心於研究工作中而毫無後顧之憂。

鑒此，謹以此篇論文獻給所有關心我的每一個人。

林育正 誌予

九十六年六月

CONTENTS

ABSTRACT (CHINESE)	I
ABSTRACT (ENGLISH)	II
ACKNOWLEDGEMENT	III
LIST OF TABLES	VI
LIST OF FIGURES	VII

CHAPTER 1 Introduction	1
-------------------------------	----------

1.1 Background and Problems.....	1
1.2 Related Works.....	3
1.3 Thesis Organization.....	3

CHAPTER 2 Basics of Microstrip Antennas	4
--	----------

2.1 Introduction of Microstrip Antennas.....	4
2.2 Basic Microstrip Antennas.....	5
2.2.1 Dipole.....	5
2.2.2 Patch Antennas.....	8
2.2.3 Slot Antennas.....	9
2.3 Architecture of Feed.....	10
2.3.1 Microstrip Line Feed.....	10
2.3.2 Probe Feed.....	11
2.3.3 Aperture Coupling Feed.....	12

2.3.4 Coplanar Waveguide Feed.....13

CHAPTER 3 Miniaturization Techniques of Microstrip Antennas 15

3.1 Patch-meandering Technique.....15

3.2 PIFA Technique.....19

3.3 Using Magneto-dielectric Materials.....21

3.4 Comparison of Three Miniaturization Techniques.....24

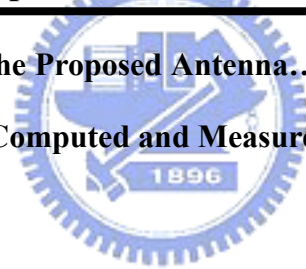
 3.4.1 Advantages of Three Miniaturization Techniques.....24

 3.4.2 Disadvantages of Three Miniaturization Techniques.....24

CHAPTER 4 The Proposed Broadband Antenna 25

4.1 Design Concept of the Proposed Antenna.....26

4.2 Comparison of the Computed and Measured results.....40



CHAPTER 5 Conclusion 56

REFERENCES.....57

List of Tables

Table 4.1	Resonant frequency comparison using Eq. (4.1) and HFSS.....	30
Table 4.2	Computed bandwidths of the planar binomial antennas.....	33
Table 4.3	The computed and measured peak gains, the radiation efficiencies of six frequencies.....	55
Table 4.4	Comparison to other published works	55



List of Figures


Figure 1.1	Some common mobile handsets of different generations.....	2
Figure 2.1	Geometry of the microstrip antenna.....	5
Figure 2.2	Geometry of the Dipole.....	7
Figure 2.3	Current distribution of the Dipole.....	7
Figure 2.4	3D polar pattern of the Dipole.....	8
Figure 2.5	Microstrip patch antenna.....	9
Figure 2.6	Geometry of the slot antenna.....	10
Figure 2.7	Geometry of the microstrip line feed network.....	11
Figure 2.8	Geometry of the probe feed network.....	12
Figure 2.9	Geometry of the aperture coupling feed network.....	13
Figure 2.10	Geometry of the coplanar waveguide feed network.....	14
Figure 3.1	Geometry of a meandered circular microstrip antenna with a shorting pin.....	17
Figure 3.2	Measured resonant frequency against slot length ℓ in the circular patch in Figure 3.1.....	17
Figure 3.3	A broadband interior antenna of planar monopole type in handsets.....	18
Figure 3.4	Computed and measured return loss of a broadband interior antenna.....	18
Figure 3.5	Current distribution of a broadband interior antenna.....	19
Figure 3.6	Geometry of a probe-fed shorted patch antenna for broadband and dual frequency operations. The dimensions given in the figure are in millimeters.....	20
Figure 3.7	Measured and computed return loss of the probe-fed shorted patch antenna shown in Figure 3.3 with a ground-plane size of $18 \times 80 \text{ mm}^2$	21

Figure 3.8	Structure of the meander line antenna using magneto-dielectric material.....	22
Figure 3.9	Return loss against permeability of pure magnetic antenna.....	23
Figure 3.10	Return loss of broadband antenna against dielectric constant.....	23
Figure 4.1	The purpose of each design step.....	26
Figure 4.2	The geometry of the simple planar rectangular antenna.....	28
Figure 4.3	The computed return loss versus frequency of the simple planar rectangular antennas.....	29
Figure 4.4	The geometry of the planar binomial antenna.....	32
Figure 4.5	The computed return loss versus frequency of the planar binomial antennas with $L_{b1} = 25 \text{ mm}$	32
Figure 4.6	The geometry of the planar hybrid-binomial antenna.....	35
Figure 4.7	The computed return loss versus frequency of the first adjustment.....	35
Figure 4.8	The geometry of the planar eagle-shaped antenna.....	37
Figure 4.9	The computed return loss versus frequency of the second adjustment.....	38
Figure 4.10	The computed current distribution of the unmodified antenna; $f = 1.575 \text{ GHz}$, $\text{phase} = 320 \text{ degrees}$	38
Figure 4.11	The computed current distribution of the modified antenna; $f = 1.575 \text{ GHz}$, $\text{phase} = 320 \text{ degrees}$	39
Figure 4.12	The computed return loss versus frequency of the planar eagle-shaped antennas by varying G	40
Figure 4.13	The geometry of the proposed antenna.....	41
Figure 4.14	The photograph of the proposed antenna.....	41
Figure 4.15	The computed and measured return loss versus frequency of the proposed antenna.....	42

Figure 4.16	The computed radiation patterns of the proposed antenna (1575 MHz)	43
Figure 4.17	The computed radiation patterns of the proposed antenna (1795 MHz)	44
Figure 4.18	The computed radiation patterns of the proposed antenna (1920 MHz)	45
Figure 4.19	The computed radiation patterns of the proposed antenna (2045 MHz)	46
Figure 4.20	The computed radiation patterns of the proposed antenna (2442 MHz)	47
Figure 4.21	The computed radiation patterns of the proposed antenna (2595 MHz)	48
Figure 4.22	The measured radiation patterns of the proposed antenna (1575 MHz)	49
Figure 4.23	The measured radiation patterns of the proposed antenna (1795 MHz)	50
Figure 4.24	The measured radiation patterns of the proposed antenna (1920 MHz)	51
Figure 4.25	The measured radiation patterns of the proposed antenna (2045 MHz)	52
Figure 4.26	The measured radiation patterns of the proposed antenna (2442 MHz)	53
Figure 4.27	The measured radiation patterns of the proposed antenna (2595 MHz)	54

Chapter 1 *Introduction*

1.1 Background and Problems



Recently, many users of mobile phones are now using mobile handsets for voice communication as well as for access into the worldwide web internet. With the rapid growth of mobile communications, there are several growing demands with handset design requirements for small, lightweight, multifunction, and multi-band. At the same time, the mobile handset adapts popularly the internal antenna structure also. Therefore, these demands for wireless terminal are an explosive issue. In microwave applications, microstrip and printed circuit antennas have many advantages such as low profile, light weight, low cost, mass production, and direct integration to with microwave circuitry.

In order to roam worldwide and to have location based services, the operation bands of major wireless services should be considered, such as the global system for mobile communication (GSM, 890–960 MHz), the global positioning system (GPS, 1575.42 MHz), digital communication system (DCS, 1710–1880 MHz), personal communication system (PCS, 1850–1990 MHz), universal mobile telecommunication

system (UMTS, 1920–2170 MHz), wireless local area network (WLAN, 2400–2484 MHz) bands [1], and worldwide interoperability for microwave access (WiMAX, 2500-2690 MHz). Thus, the design and implementation of such a wide-band antenna accordingly with integrated wireless communication services become a significant topic.

Figure 1.1 shows the common mobile handsets of different generations. The bar shaped mobile phones are shown in Fig. 1.1 (a) to 1.1 (c). The flip phones are shown in Fig. 1.1 (d) to 1.1 (f). We also find that external antennas are disappeared in the newer mobile phones such as (b) (c), (e) and (f). From these pictures, we find that to fit the pocket size, handsets are getting thinner and smaller.



Figure 1.1 Some common mobile handsets of different generations.

(a) Nokia 6150 (b) Nokia 3210 (c) Motorola L6

(d) Motorola V3688x (e) Motorola V80 (f) Motorola V3

1.2 Related Works

There are many works reported on multi-band and broadband antennas for mobile handsets [1]–[9]. Most of internal antennas reported so far are planar antennas [1]–[3], meander-line antennas [4]–[5], and planar inverted F-Antennas (PIFA) [6]–[9]. The planar monopole antennas [1]–[3] are printed on a substrate by easy processing, and that has a simple structure. Although it has a small size, there is a limit to obtain the broadband characteristic. For the meander-line antennas [4]–[5], although it is very small size, its fabrication is difficult so that the production cost is very high. For the PIFA [6]–[9], there are advantages of low profile, compact size, and multiple-band operations for mobile phones. However, it suffers from narrow bandwidth and limitation in antenna height (6–8 mm) to obtain the desired results. In addition, the PIFA antenna cannot easily be placed on the substrate of a practical mobile phone.

1.3 Organization of Thesis

The thesis is organized as follows. In Chapter 2, some basic microstrip antennas are presented shortly and three feeding structures are also introduced in this chapter. In Chapter 3, three popular miniaturization techniques are presented from some literatures. The comparisons of three miniaturization techniques are also listed in this chapter. Chapter 4 presents the proposed antenna and investigates the effect of the geometrical parameters of the antenna. Then, numerical and measured results of the proposed antenna are also shown in this chapter. Finally, Conclusion is drawn in Chapter 5.

Chapter 2 *Basics of Microstrip Antennas*

2.1 Introduction of Microstrip Antennas

A microstrip structure in its simplest form as illustrated in Figure 2.1 is a layered structure with two parallel conductors separated by a thin dielectric substrate and the lower conductor acting as a ground plane. If the upper metallization is a long narrow strip, a microstrip transmission line is formed. If the upper conductor is a patch that is an appreciable fraction of a wavelength in extent, the structure becomes a microstrip antenna [10]. Microstrip antennas mainly radiate electromagnetic waves from upper conductors. Many conventional structures of antennas can be applied to microstrip antennas. Because microstrip antennas have a very low profile, are mechanically rugged and can be conformable, they are often incorporated into mobile radio communications devices. Some basic microstrip antennas are described as followings.

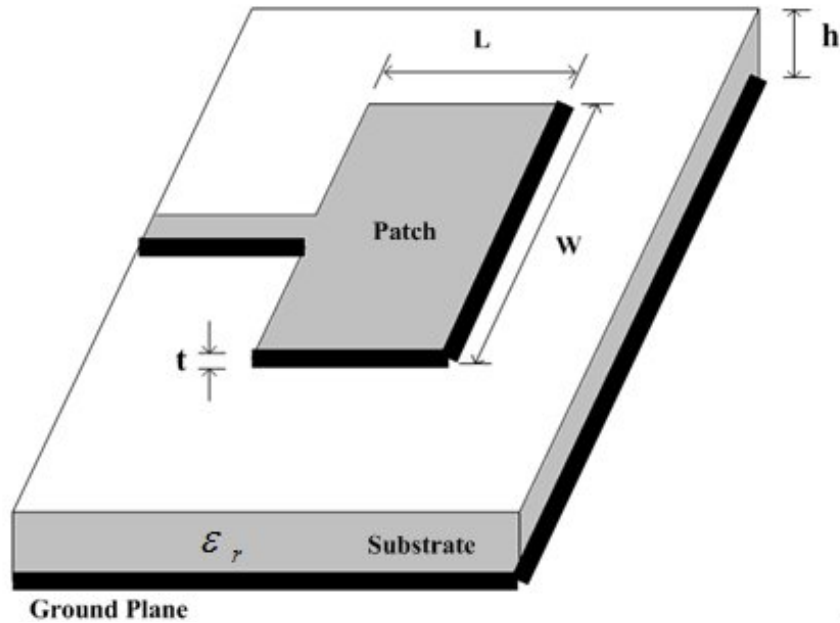


Figure 2.1 Geometry of the microstrip antenna.

2.2 Basic Microstrip Antennas

2.2.1 Dipole

The dipole is a common antenna. A very widely used antenna is the half-wave dipole antenna. It is a linear current whose amplitude varies as one-half of a sine wave with a maximum at the center. Because its radiation resistance is 73 ohms, which is very near the 50-ohm or 75-ohm characteristic impedance of some transmission lines, its matching to the line is simplified especially at resonance. The advantage of a half-wave dipole is that it can be made to resonate and present a zero input reactance, thus eliminating the need for tuning to achieve a conjugate impedance match [10], a half-wavelength dipole is illustrated in Figure 2.2.

The length of the dipole is $\frac{\lambda}{2}$. In fact, the physical length must be somewhat shorter than a free space half-wavelength. As usual, the current distribution is placed along the z-axis and for the half-sine wave current on the half-wave dipole, the current

distribution is written as

$$I(z) = I_m \sin\left[\beta\left(\frac{\lambda}{4} - |z|\right)\right], \quad |z| \leq \frac{\lambda}{4} \quad (2.1)$$

where $\beta = \frac{2\pi}{\lambda}$. This current goes to zero at the ends (for $z = \pm \frac{\lambda}{4}$) and its maximum value

I_m occurs at the center ($z = 0$) as shown in Figure 2.3. From this current, we can

calculate the radiation pattern. Since it is a z-directed line source, we can use

$$A = \hat{z}\mu \frac{e^{-j\beta r}}{4\pi r} \int I(z') e^{j\beta z' \cos\theta} dz' \quad (2.2)$$

$$E = -j\omega A \quad (2.3)$$

$$E = -j\omega A - (-j\omega A \cdot \hat{r})\hat{r} = -j\omega(A_\theta \hat{\theta} + A_\phi \hat{\phi}) \quad (2.4)$$

$$E = -j\omega \sin\theta A_z \hat{\theta} \quad (2.5)$$

to find the electric field as

$$E_\theta = j\omega\mu \sin\theta \frac{e^{-j\beta r}}{4\pi r} \int I(z') e^{j\beta z' \cos\theta} dz' \quad (2.6)$$

Substituting $I(z)$ into the integration and evaluating gives

$$E_\theta = j\omega\mu \frac{2I_m}{\beta} \frac{e^{-j\beta r}}{4\pi r} \sin\theta \frac{\cos\left[\left(\frac{\pi}{2}\right)\cos\theta\right]}{\sin^2\theta} \quad (2.7)$$

In this expression, we can identify the element factor $g(\theta) = \sin\theta$ and the normalized pattern factor

$$f(\theta) = \frac{\cos\left[\left(\frac{\pi}{2}\right)\cos\theta\right]}{\sin^2\theta} \quad (2.8)$$

Both $g(\theta)$ and $f(\theta)$ are maximum for $\theta = \frac{\pi}{2}$ and have a value of unity there. The

complete (normalized) far-field pattern is then

$$F(\theta) = g(\theta)f(\theta) = \frac{\cos\left[\left(\frac{\pi}{2}\right)\cos\theta\right]}{\sin\theta} \quad (2.9)$$

The half-wave dipole has a narrower beamwidth of 78° , and thus, a higher directivity

value of 1.64 [10]. The 3D polar pattern of a half-wavelength dipole is shown in Figure 2.4.

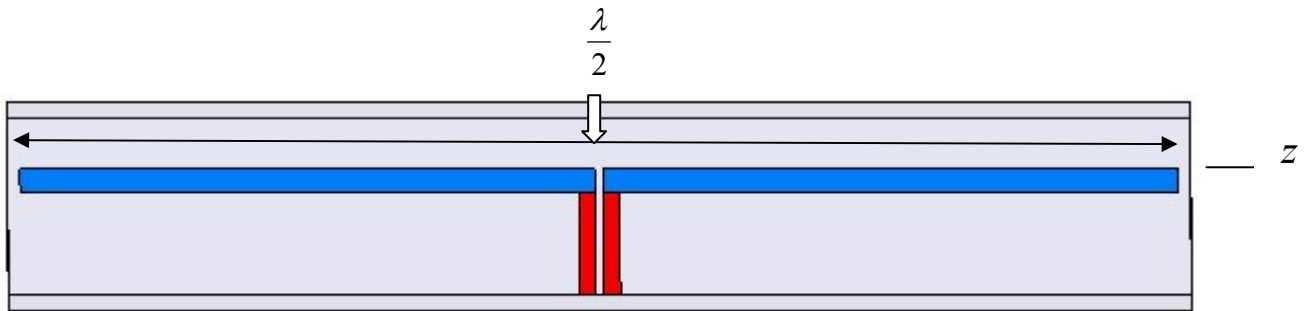


Figure 2.2 Geometry of a half-wavelength dipole.

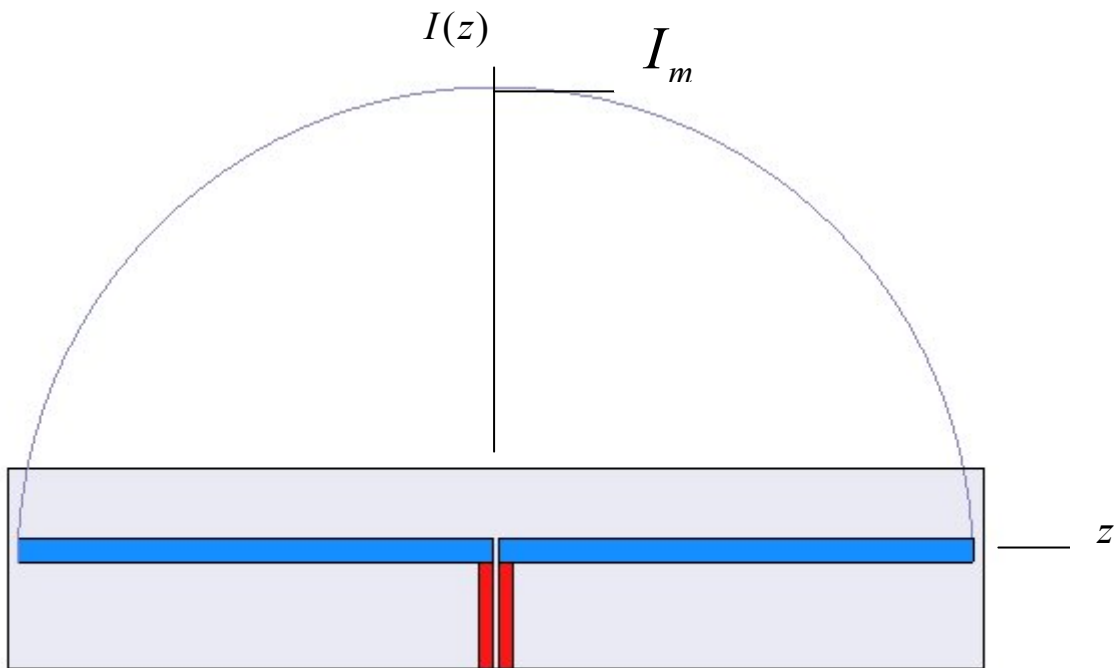


Figure 2.3 Current distribution of a half-wavelength dipole.

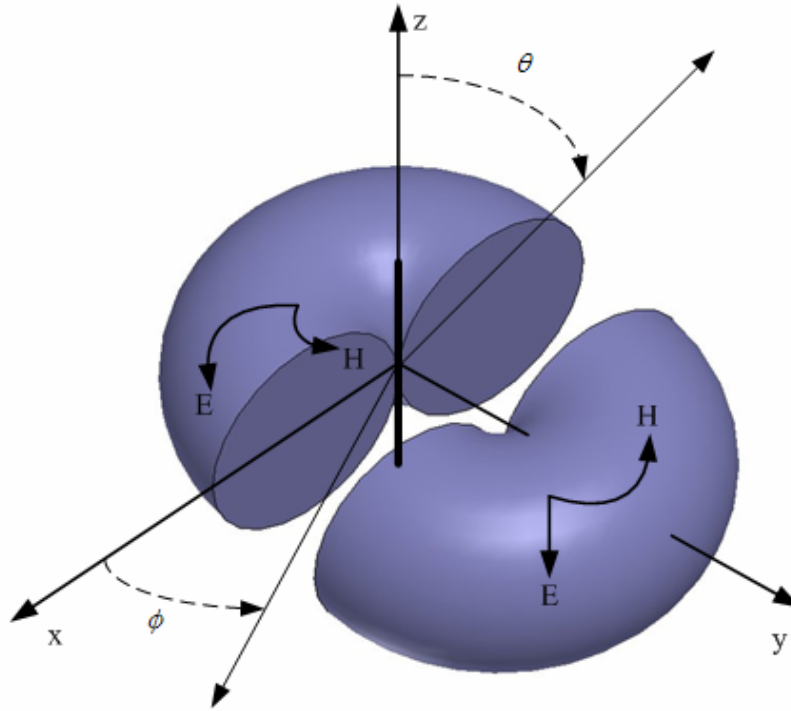


Figure 2.4 3D polar pattern of a half-wavelength dipole.

2.2.2 Patch Antennas

The rectangular patch is the most widely used configuration. Because of the fringing effects, electrically the patch of the microstrip antenna looks greater than its physical dimensions. For the principle E-plane (x-y plane), this is demonstrated in Figure 2.5 where the dimensions of the patch along its length have been extended on each end by a distance ΔL , which is a function of the effective dielectric constant $\epsilon_{r_{eff}}$ and the width-to-height ratio $(\frac{W}{h})$. For the dominant TM_{010} mode, the resonant frequency of the microstrip antenna is a function of its length. Usually it is given by [10]

$$(f_r)_{010} = \frac{1}{2L\sqrt{\epsilon_r}\sqrt{\epsilon_0\mu_0}} = \frac{v_0}{2L\sqrt{\epsilon_r}} \quad (2.10)$$

v_0 is the speed of light in free space.

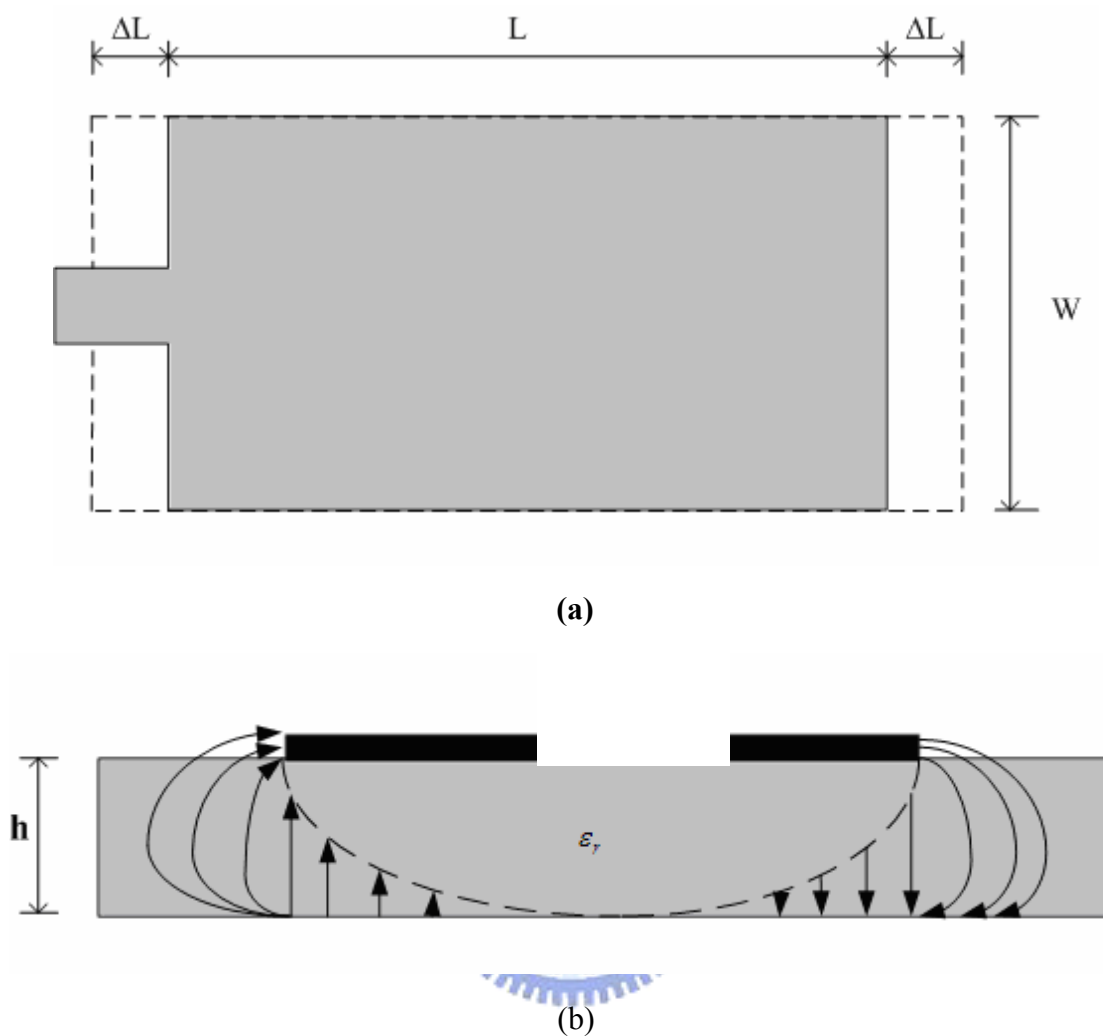


Figure 2.5 Microstrip patch antenna (a) Top view (b) Side view.

2.2.3 Slot Antennas

By embedding suitable slots in the radiation patch of a microstrip antenna, enhanced bandwidth with a reduced antenna size can be obtained. This can be accomplished by increasing the number of resonances of single resonant antennas such as a half-wavelength slot. An example is illustrated in Figure 2.6. It is found that, by embedding a pair of branchlike slots of proper dimensions, the first two broadside-radiation modes TM_{10} and TM_{20} of the triangular microstrip antenna can be perturbed such that their resonant frequencies are lowered and close to each other to

form a wide impedance bandwidth [11].

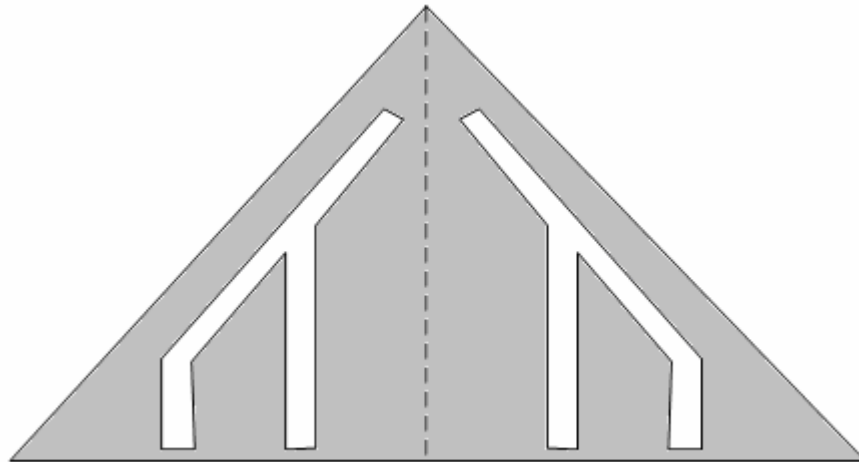


Figure 2.6 Geometry of the slot antenna.

2.3 Architectures of Feed

There are many configurations that can be used to feed microstrip antennas. The four most popular architectures of feed are microstrip line feed, probe feed, aperture coupling feed, and coplanar waveguide feed [10].

2.3.1 Microstrip Line Feed

The microstrip line feed network is illustrated in Figure 2.7 [10]. The microstrip line feed is easy to fabricate, simple to match by controlling the inset position and rather simple to model. However, as the substrate thickness increases, surface wave and spurious feed radiation increase, which for practical designs limit the bandwidth.

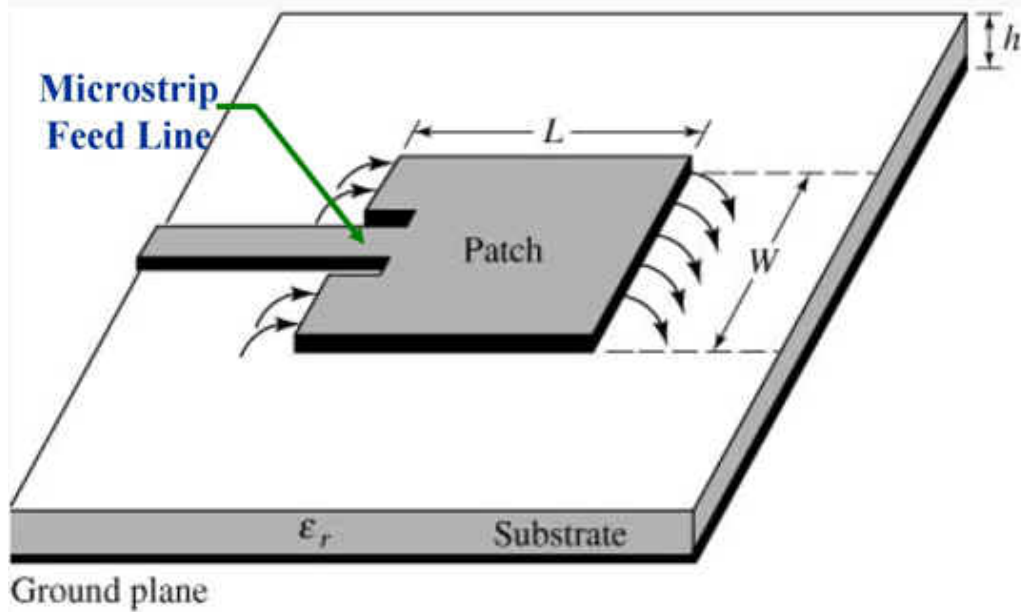


Figure 2.7 Geometry of the microstrip line feed network.

2.3.2 Probe Feed

The probe feed is illustrated in Figure 2.8 [10]. Probe feed, where the inner conductor of the coax is attached to the radiation patch while the outer conductor is connected to the ground plane, are also widely used. The coaxial probe feed is also easy to fabricate and match, and it has low spurious radiation, However, it is also has narrow bandwidth and it is difficult to model, especially for thick substrates ($h > 0.02\lambda_0$).

Both the microstrip line and the probe feed possess inherent asymmetries which generate higher order modes which produce cross-polarized radiation. To overcome these problems, no contacting aperture coupling feed is used [10].

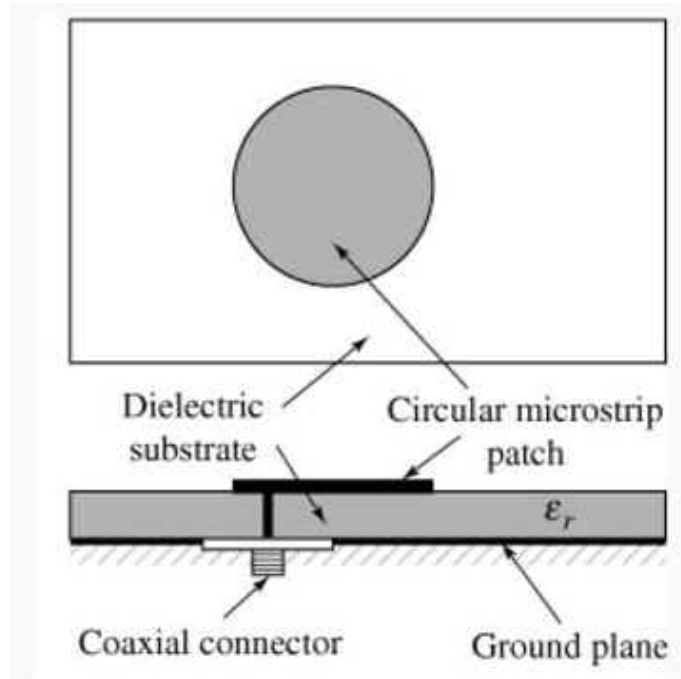


Figure 2.8 Geometry of the probe feed network.

2.3.3 Aperture Coupling Feed

The aperture coupling feed is illustrated in Figure 2.9 [10]. The aperture coupling feed is the most difficult of all feeding methods to fabricate and it also has narrow bandwidth. However, it is somewhat easier to model and has moderate spurious radiation. The aperture coupling feed consists of two substrates separated by ground plane. On the bottom side of the lower substrate there is a microstrip feed line whose energy is coupled to the patch through a slot on the ground plane separating the two substrates. This arrangement allows independent optimization of the feed mechanism and the radiating element. Typically a high dielectric material is used for the bottom substrate. The ground plane between the substrates also isolates the feed from the radiating element and minimizes interference of spurious radiation for pattern formation and polarization purity. Typically matching is performed by controlling the width of the feed line and the length of the slot.

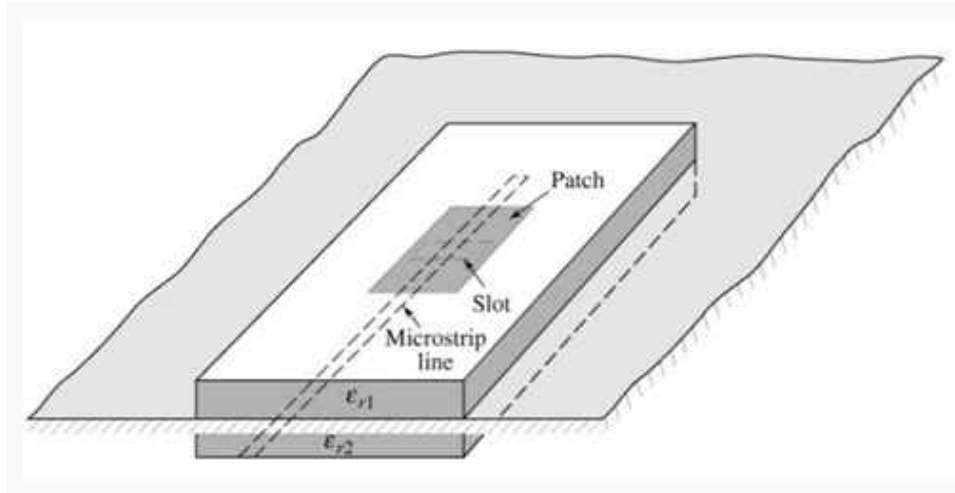
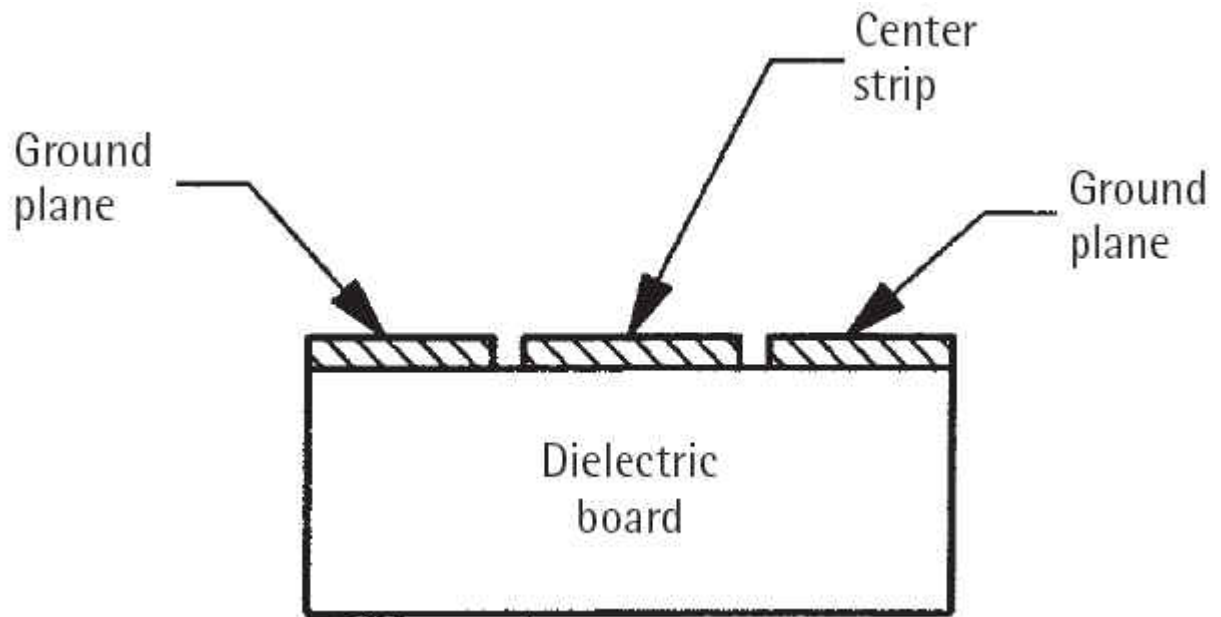


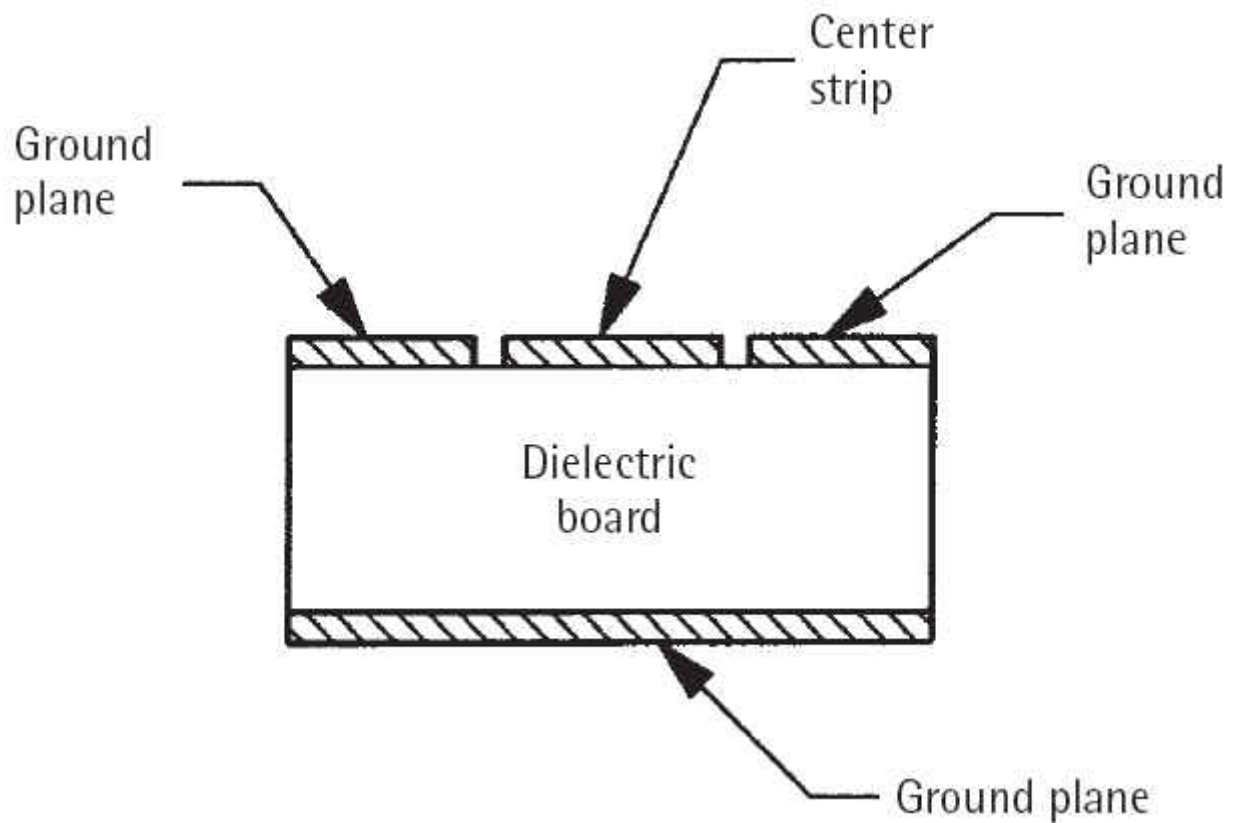
Figure 2.9 Geometry of the aperture coupling feed network.

2.3.4 Coplanar Waveguide Feed

The coplanar waveguide feed is illustrated in Figure 2.10 [12]. The coplanar waveguide feed is widely used in industry and investigated in academia for a long time. It is an important transmission line. The advantages of coplanar waveguide feed are low radiation loss, wide bandwidth, easy to integrate to MIC or MMIC, and simple to tune the characteristic impedance by changing the ratio of the slit width and the microstrip line width. In order to the coplanar architecture, it is not necessary to dig holes for parallel or series to active elements.



(a)

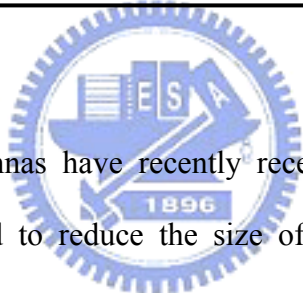


(b)

Figure 2.10 Geometry of the coplanar waveguide feed network

(a) Coplanar waveguide (b) Ground backed coplanar waveguide.

Chapter 3 *Miniaturization Techniques of Microstrip Antennas*



Compact microstrip antennas have recently received much attention and many techniques have been reported to reduce the size of microstrip antennas at a fixed operating frequency such as [11]-[14]. The popular techniques include patch-meandering technique, PIFA technique, and using magneto-dielectric materials. They are described as followings:

3.1. Patch-meandering Technique

This kind of patch-meandering technique is achieved mainly by creating several meandering slits at the non-radiating edges of a rectangular patch or at the boundary of a circular patch [13]. The characteristics of patch-meandering technique are compact and broadband. Compact operation of microstrip antennas can be obtained by meandering the radiating patch. Broadband characteristic can be accomplished by increasing the number of resonances of single resonant antennas such as a

half-wavelength meandering patch.

In the following, a compact design combining the techniques of patch meandering and shorting-pin loading for a circular microstrip antenna is demonstrated. Figure 3.1 [11] shows the geometry of a short-circuited, meandered circular microstrip antenna. The circular patch is short-circuited at the edge with a shorting pin, and three narrow slots of the same length ℓ and width w are cut in the patch. The shorting pin makes the circular patch resonate at a much lower frequency compared with a conventional circular patch of the same size, and the narrow slots meander the patch, which increases the effective electrical length of the patch. These two factors effectively reduce the required disk size for an antenna operated at a given frequency. Figure 3.2 [11] shows the measured resonant frequency against slot length ℓ in Figure 3.1. As $\ell/2R$ increases, the resonant frequency decreases to a lower frequency. Thus, it is obviously realized that the patch-meandering technique is a good method for miniaturization of microstrip antennas.

Figure 3.3 [4] shows a broadband interior antenna with a meandering structure. The broadband frequency response is shown in Figure 3.4 [4] and the current distribution in the resonant frequency of the antenna is shown in Figure 3.5 [4]. From Figure 3.5, it is obviously seen that there are three current paths in this antenna. Thus, the broadband characteristic can be arrived by proper design of the length of each current path. In this case, it is known that the broadband antenna can be designed by a meandering structure.

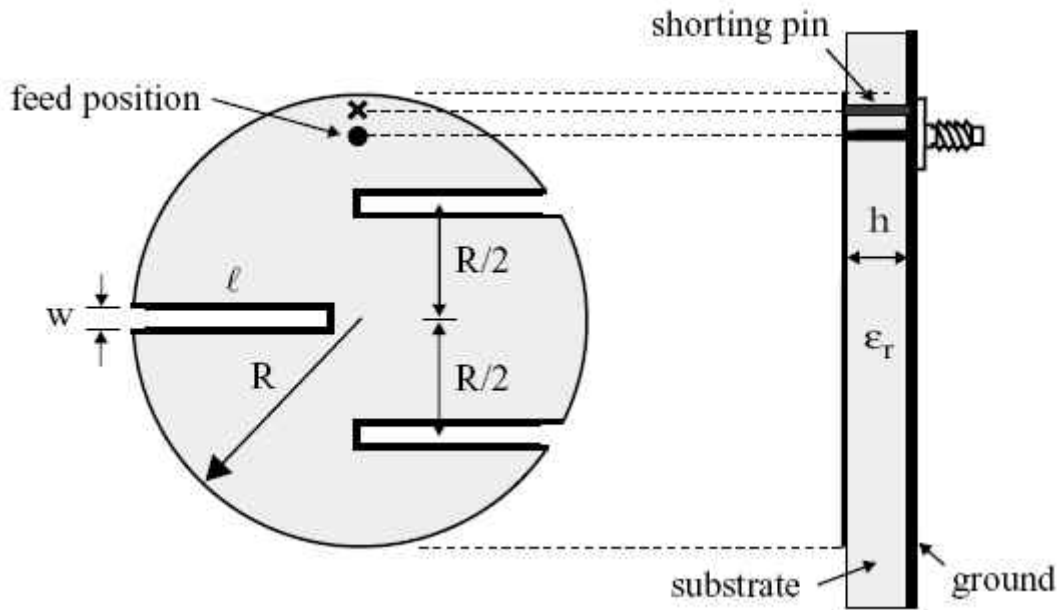


Figure 3.1 Geometry of a meandered circular microstrip antenna with a shorting pin.

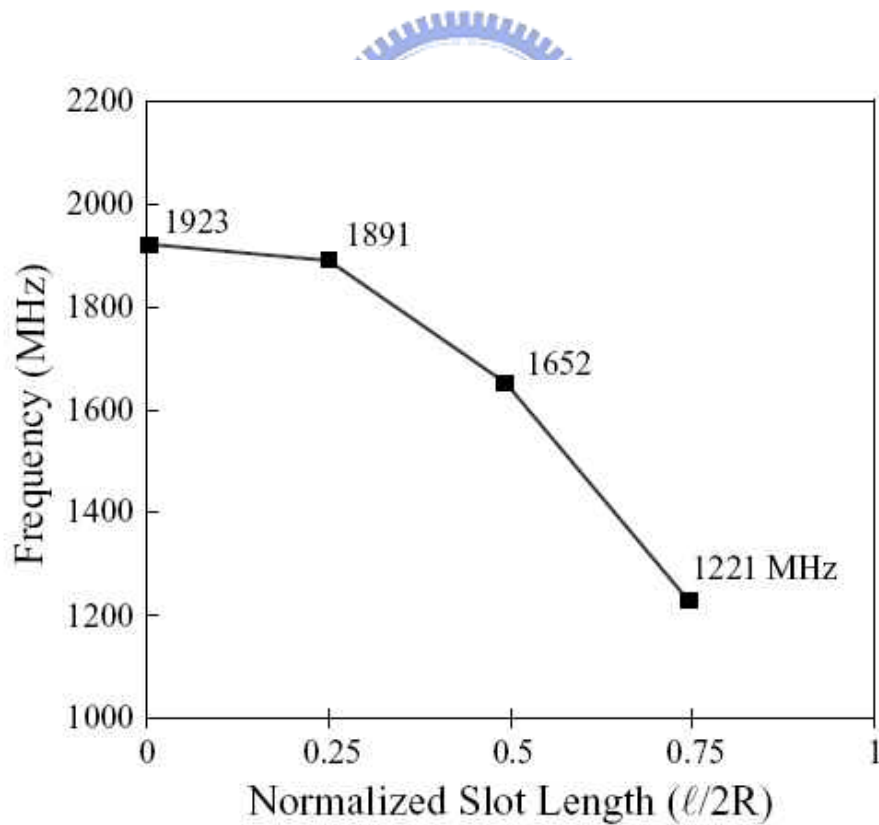


Figure 3.2 Measured resonant frequency against slot length l in the circular patch in

Figure 3.1; $R=7.5$ mm, $d_s=6.5$ mm.

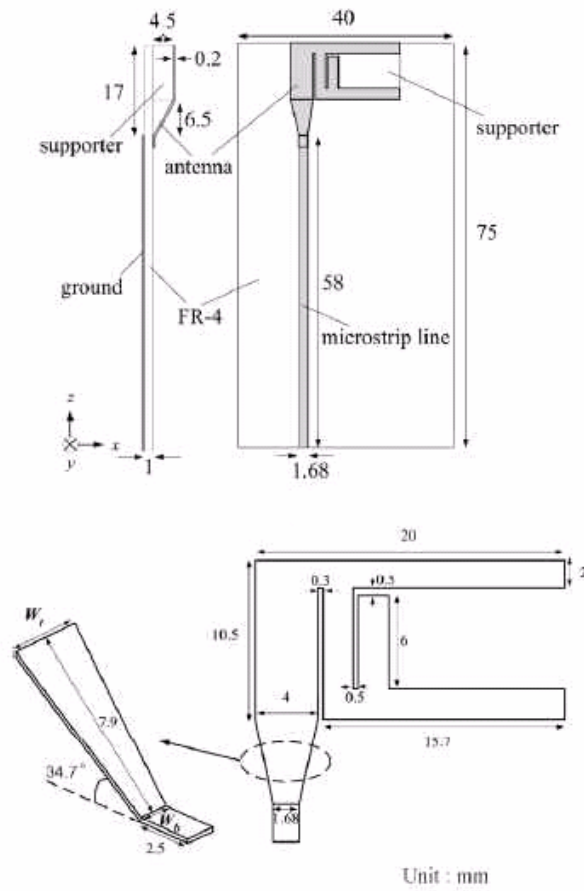


Figure 3.3 A broadband interior antenna of planar monopole type in handsets.

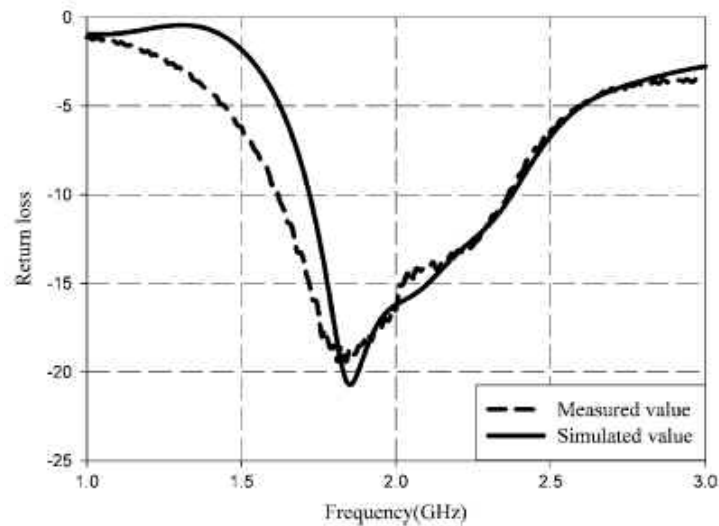


Figure 3.4 Simulated and measured return loss of a broadband interior antenna.

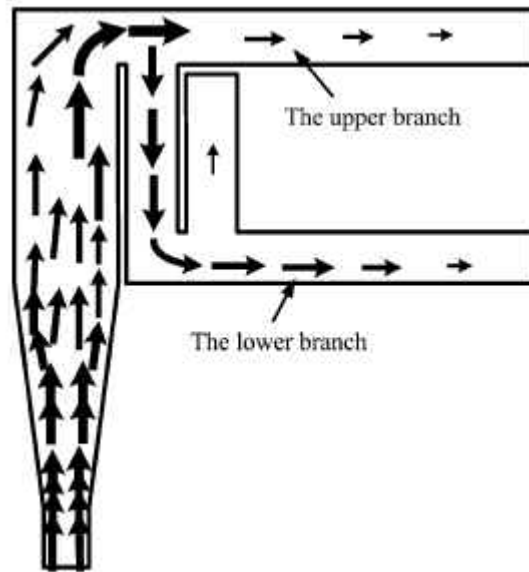


Figure 3.5 Current distribution of a broadband interior antenna.

3.2 PIFA Technique

Effective resonant length of an antenna can be shortened by applying PIFA technique. Figure 3.6 shows a typical design example for a probe-fed shorted patch antenna operated at dual bands of 1.8 and 2.45 GHz. A shorting strip of width 2.5 mm is used for short-circuiting the rectangular patch to the ground plane. The geometry of this structure looks like a planar inverted F. So this structure of antennas is called PIFA (Planar inverted F antenna). Between the rectangular radiating patch and the ground plane is an air substrate of thickness 9.6 mm. The rectangular patch has dimensions of $36 \times 16 \text{ mm}^2$, an L-shaped slit of width 1 mm and total length 40 mm is cut in the rectangular patch for achieving an additional operating band at 2.45 GHz (the industrial, scientific, medical [ISM] band); the lower operating band at 1.8 GHz is mainly controlled by the dimensions of the rectangular patch [11]. The simulation and measurement results are shown in Figure 3.7. [11] IE3D is the simulator. In this example, it can be seen that the longer patch length corresponds to the lower resonant

frequency is about $\frac{\lambda}{4}$ of the lower center frequency. In conventional cases, the resonant length is about $\frac{\lambda}{2}$ of the center frequency. In the same manner, the shorter patch length corresponds to the higher resonant frequency is about $\frac{\lambda}{4}$ of the higher center frequency. It can be obviously seen that the antenna size is greatly decreased. So the PIFA technique is the very popular design guide for the designs of the mobile handsets. It is widely used in the new thin and small handsets.

From Figure 3.7, the bandwidth of the lower resonant is 302 MHz (1588-1890 MHz). The wide bandwidth is just because the multiple current paths can be selected by a roomy radiating element.

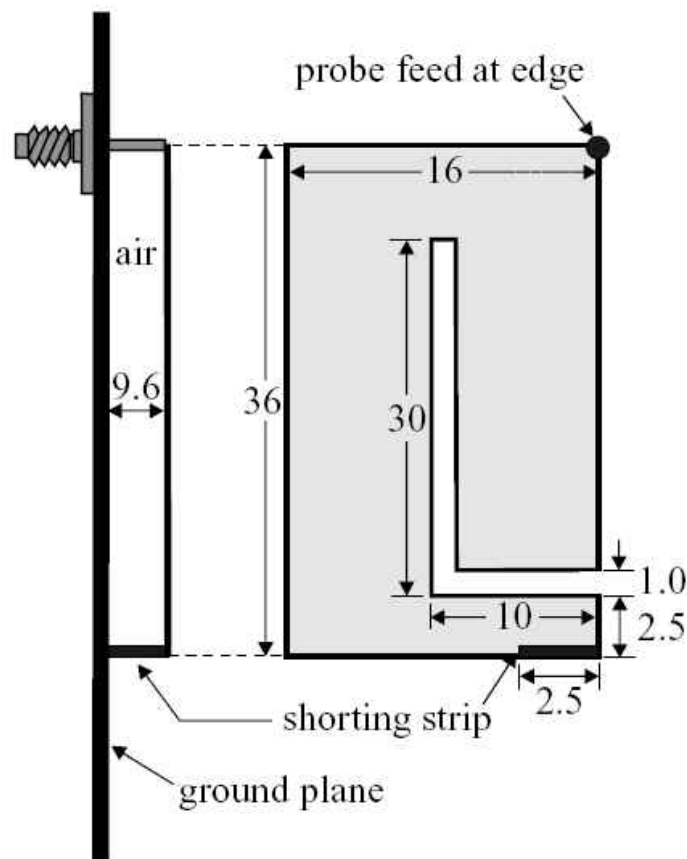


Figure 3.6 Geometry of a probe-fed shorted patch antenna for broadband and dual frequency operations. The dimensions given in the figure are in millimeters.

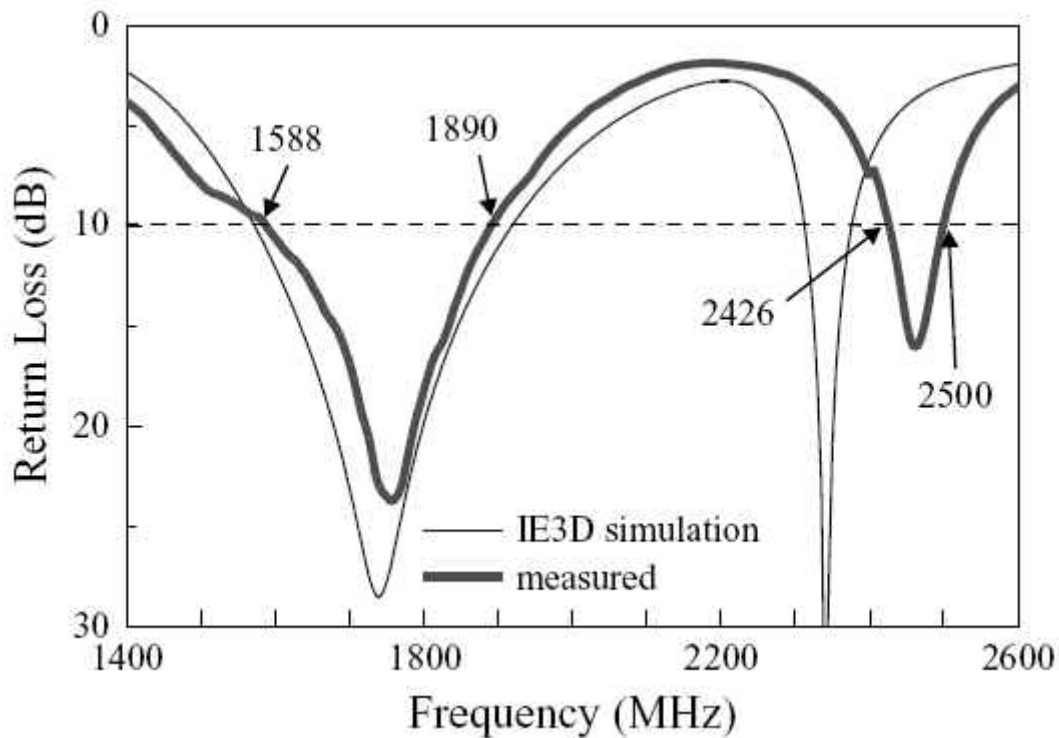


Figure 3.7 Measured and simulated return loss of the probe-fed shorted patch antenna shown in Figure 3.3 with a ground-plane size of $18 \times 80 \text{ mm}^2$.

3.3 Using Magneto-dielectric Materials

The magneto-dielectric material is utilized for broadening the bandwidth and minimizing the size of antenna. Figure 3.8 [14] shows the design of meander line antenna that is developed to get broadband characteristic with small size. This is done by accompanied with using magnetic material as the dielectric substrate. [14] In this design, the changing factors are permeability and permittivity. The Figure 3.9 [14] shows the return loss against permeability of pure magnetic antenna. It can be seen that the resonant frequency will be changed by changing the permeability. It is not only used for reducing the sizes, but also for adjusting resonant frequency. In the same manner, The Figure 3.10 [14] shows the return loss of broadband antenna against dielectric constant. The resonant frequency will be changed by different permittivity. It also can

be used to reduce sizes and adjust resonant frequency. This design is also a broadband structure. So the magneto-dielectric material is used to achieve broadband and miniaturization characteristics.

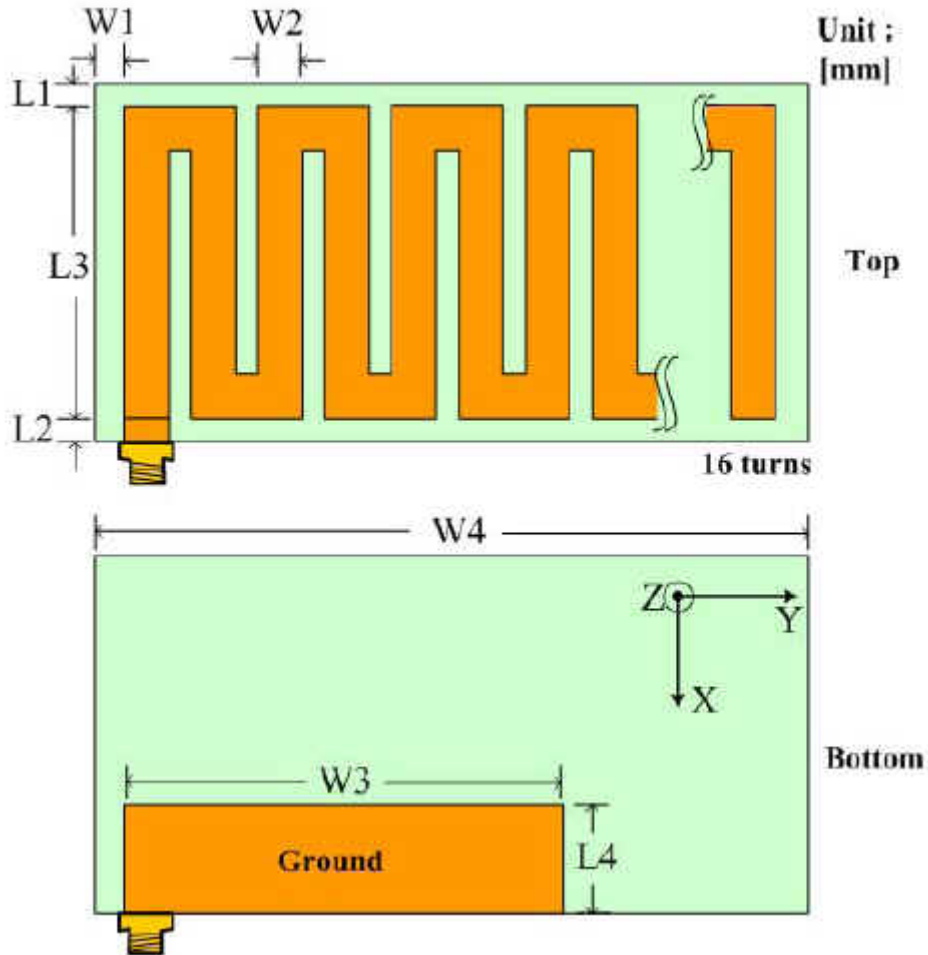


Figure 3.8 Structure of the meander line antenna using magneto-dielectric material.

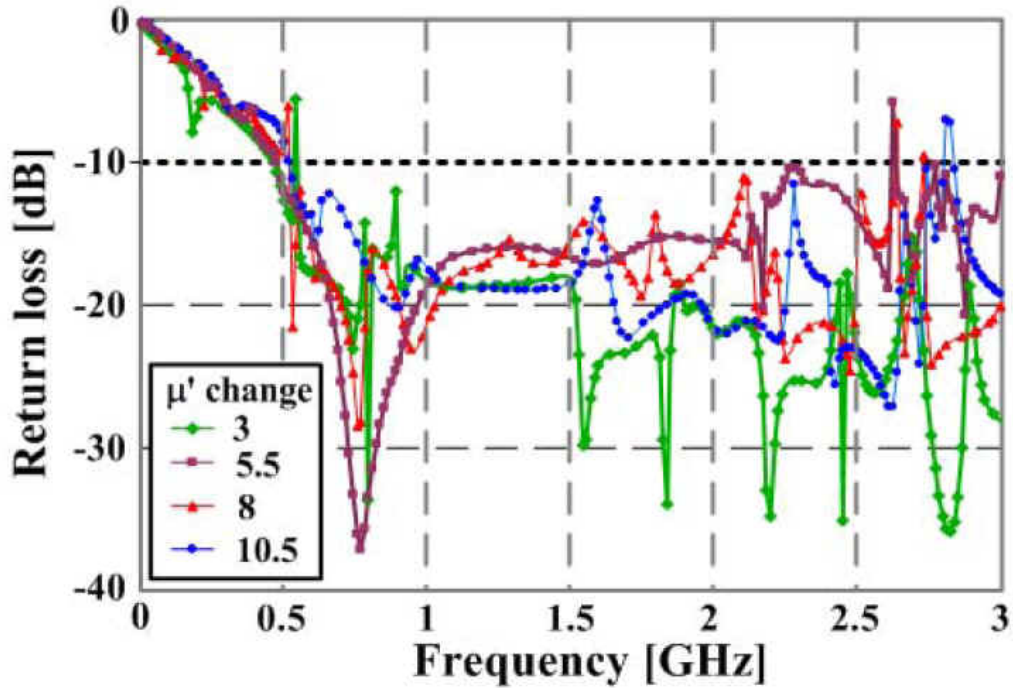


Figure 3.9 Return loss against permeability of pure magnetic antenna

(Antenna parameters: $L_1 = 0.5$ mm, $L_2 = 1$ mm, $L_3 = 9.5$ mm, $L_4 = 4$ mm, $W_1 = 1.8$ mm, $W_2 = 1$ mm, $W_3 = 35$ mm, $W_4 = 50$ mm, $\mu'' = 2$, $\epsilon'' = 2$).

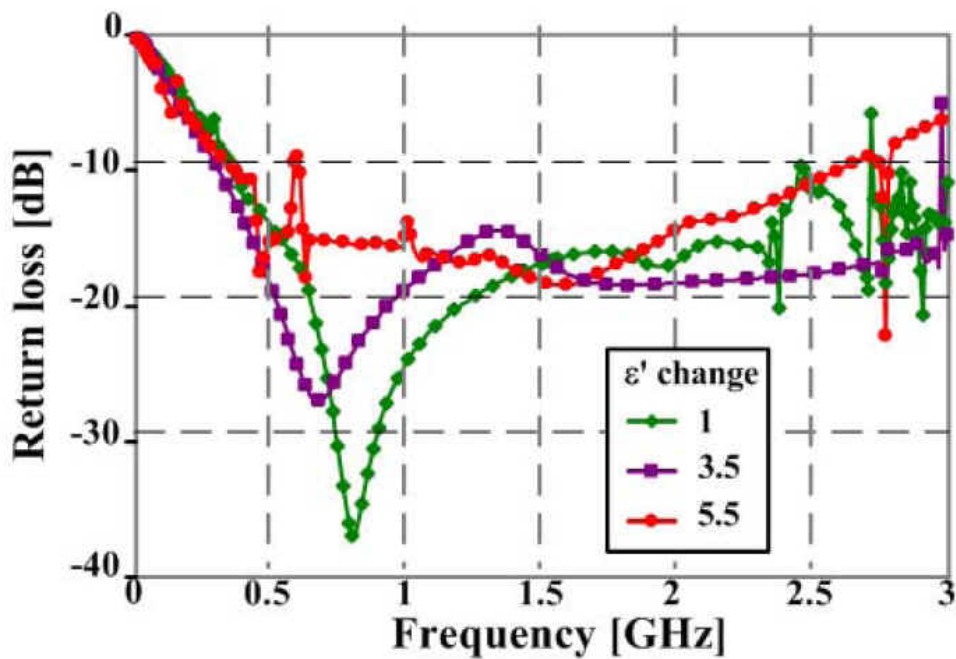


Figure 3.10 Return loss of broadband antenna against dielectric constant.

3.4 Comparison of Three Miniaturization Techniques

3.4.1 Advantages of Three Miniaturization Techniques

In this chapter, three miniaturization techniques are introduced. Patch-meandering technique can be obtained a very small size and broadband bandwidth by proper design. Its advantages are low profile, small size, low cost, easily fabricated. Comparing with conventional structures, effective resonant length can be reduced nearly a half by PIFA technique. Its advantages are low profile, small size, low cost, easily fabricated and it can be also arrived the broadband characteristic by proper design. Different characteristics of antennas will appear by using magneto-dielectric materials. Its advantages are low profile, small size, broad bandwidth, adjustable frequency.

3.4.2 Disadvantages of Three Miniaturization Techniques

The disadvantages of patch-meandering technique are low gain, hard to design. Because of coupling effect in the adjacent lines, the energy will be storing in the coupling capacitance. The radiation efficiency will decrease to a low level. The disadvantages of PIFA technique are hard to design, low radiation efficiency, low gain. Because the current flows on PCB, the energy loss and lower radiation efficiency will occur. The disadvantages of using magneto-dielectric materials are more expensive, hard to fabricate, low gain.

Chapter 4 *The Proposed Broadband Antenna*

The proposed antenna is suitable for multi-band operations covering the bands of GPS (1575.42 MHz), GSM (1710–1880 MHz), PCS (1850–1990 MHz), 3G (1920–2170 MHz), WLAN (2400–2484 MHz), and WiMAX (2500–2690 MHz). The antenna is a planar antenna on a substrate, which is small enough to be installed in mobile handsets.

4.1 Design Concept of the Proposed Antenna

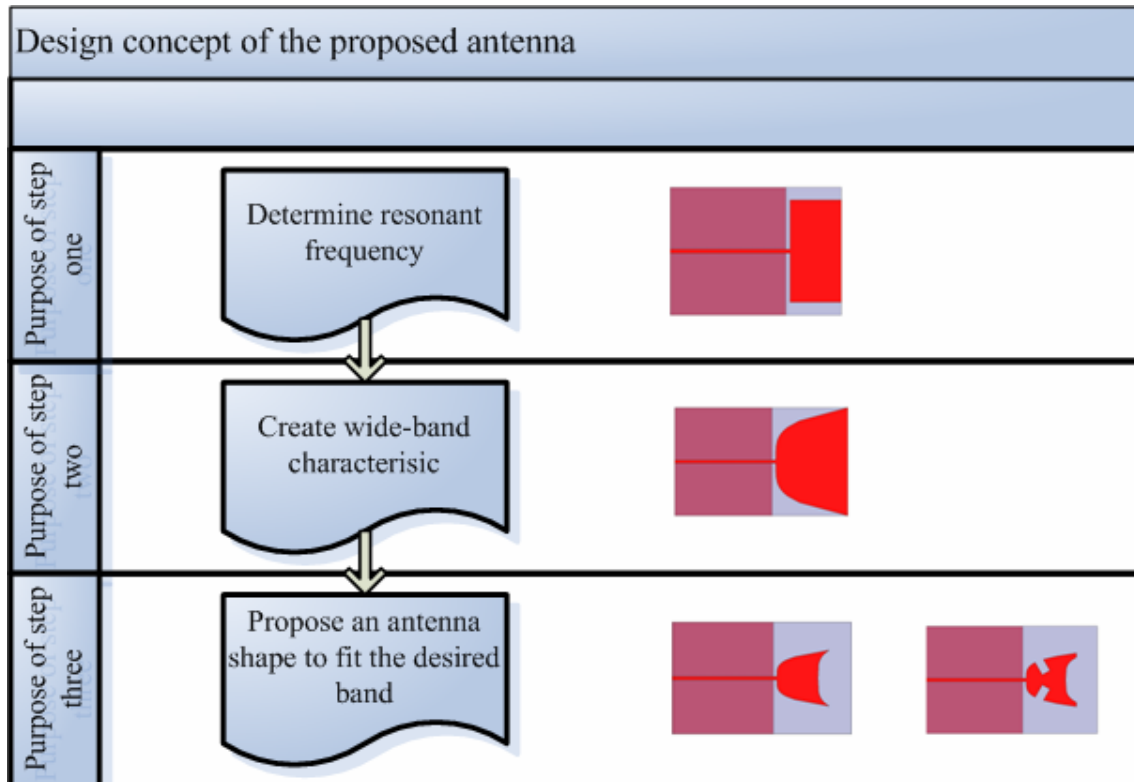


Figure 4.1 The purpose of each design step.

The design purpose of each major step is shown in Figure 4.1. In step one, the main work is to determine the rough dimension of the antenna according to the required center frequency. In step two, the broadband characteristic was created. In step three, the work is to match the desired frequency band by adjusting the geometrical parameters of the antenna. In step four, coupling effects between the ground plane and the antenna was discussed. In all steps, FR4 with thickness of 0.8 mm is used for computing by HFSS. Width of the feed line is 1.5 mm.

Step One : Determine the rough dimension of the antenna according to the required center frequency

The resonant (center) frequency of the simple planar rectangular antenna shown in Figure 4.2 is given by [16]

$$f_r \approx \frac{72}{L_r + 0.25W_r + 1} \text{ (GHz)} \quad (4.1)$$

Here, W_r (mm) and L_r (mm) are the width and length of the rectangular patch, respectively, as shown in Figure.4.2. The wanted center frequency will be achieved by properly tuning L_r and W_r . The computed results using Eq. (4.1) and HFSS are compared in Table 4.1 (Up to 4GHz) for different combinations of L_r and W_r . Here, $W = 50$ mm, $L = 45$ mm and $G = 1.6$ mm are fixed for simplification. The comparison shows that Eq. (4.1) at least determines one of resonant frequencies with reasonable accuracy. Therefore, Eq. (4.1) is proposed as a rough model for determining the resonant frequency of the simple patch antenna. Sizes of L_r and W_r will affect the bandwidth of the planar rectangular antenna. Figure 4.3 (a), (b) and (c) show its return loss versus frequency for $W_r = 25$ mm, 35 mm and 45 mm, respectively. In each figure, it is found that the bandwidth is increased with L_r . It is also found that when $W_r = 25$ mm, more than one resonant frequency may be created. In Table 4.1, the one of specific size of L_r and W_r , which are underlined, represents its resonant frequencies in the range of 1.7 - 1.8 GHz to fulfill the desired bands.

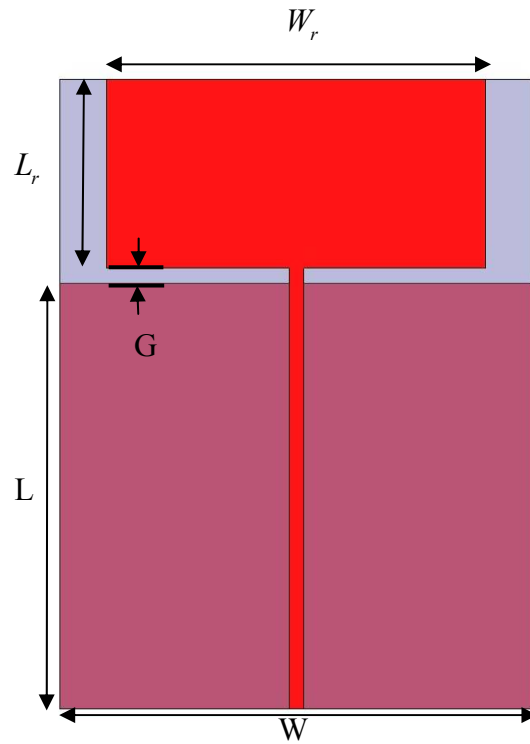
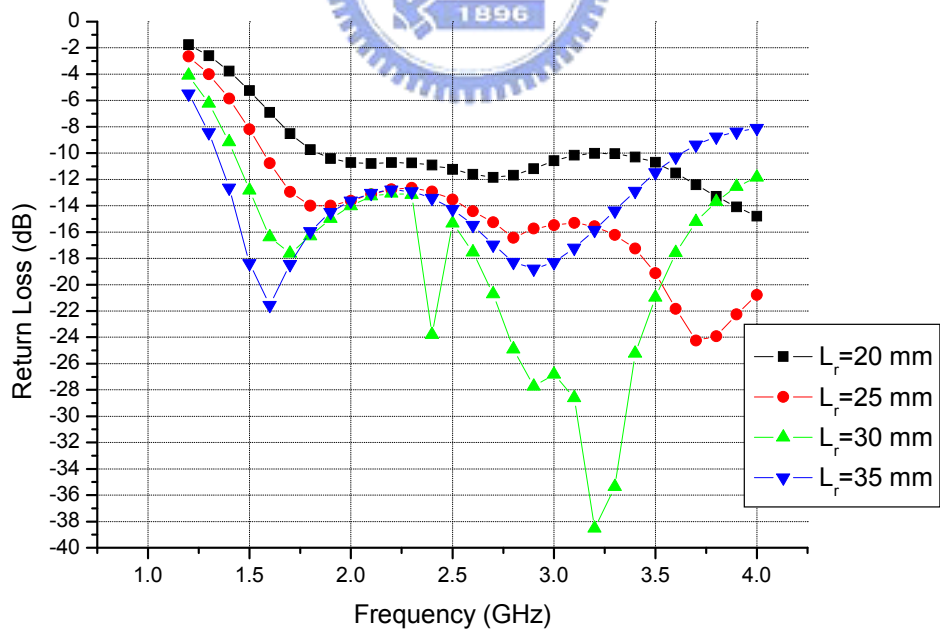
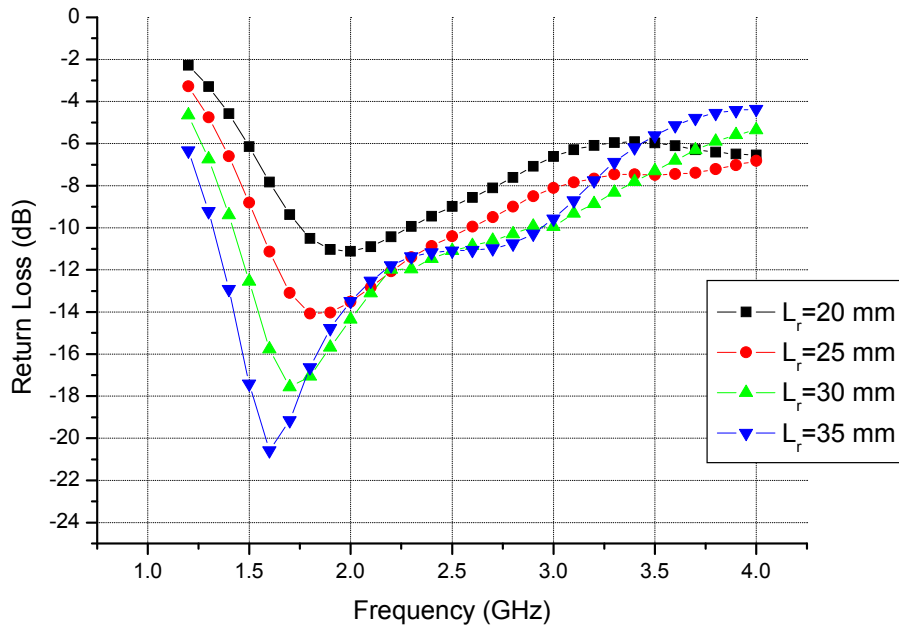


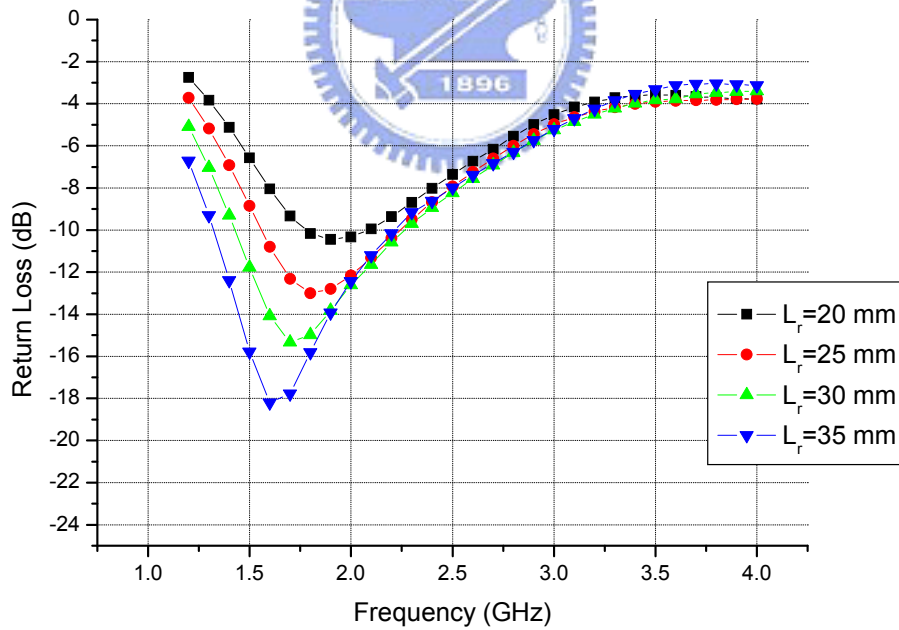
Figure 4.2 The geometry of the simple planar rectangular antenna.



(a) $W_r = 25 \text{ mm}$



(b) $W_r = 35 \text{ mm}$



(c) $W_r = 45 \text{ mm}$

Figure 4.3 The computed return loss versus frequency of the simple planar rectangular antennas (a) $W_r = 25 \text{ mm}$ (b) $W_r = 35 \text{ mm}$ (c) $W_r = 45 \text{ mm}$.

Table 4.1 Resonant frequency comparison using Eq. (4.1) and HFSS.

Computed resonant frequency W_r / L_r (mm/mm)	using Eq.(4.1)	using HFSS
25/20	2.64 GHz	2.7/4.0 GHz
<u>25/25</u>	<u>2.23 GHz</u>	<u>1.8/2.8/3.7 GHz</u>
<u>25/30</u>	<u>1.93 GHz</u>	<u>1.7/2.4/3.2 GHz</u>
25/35	1.70 GHz	1.6/2.9 GHz
30/20	2.53 GHz	2 GHz
<u>30/25</u>	<u>2.15 GHz</u>	<u>1.8 GHz</u>
<u>30/30</u>	<u>1.87 GHz</u>	<u>1.7 GHz</u>
30/35	1.66 GHz	1.6 GHz
35/20	2.42GHz	2.0GHz
<u>35/25</u>	<u>2.07GHz</u>	<u>1.8GHz</u>
<u>35/30</u>	<u>1.81GHz</u>	<u>1.7GHz</u>
35/35	1.61GHz	1.6GHz
40/20	2.32GHz	1.9GHz
<u>40/25</u>	<u>2.00GHz</u>	<u>1.8GHz</u>
<u>40/30</u>	<u>1.76GHz</u>	<u>1.7GHz</u>
40/35	1.57GHz	1.6GHz
45/20	2.23GHz	1.9GHz
<u>45/25</u>	<u>1.93GHz</u>	<u>1.8GHz</u>
<u>45/30</u>	<u>1.70GHz</u>	<u>1.7GHz</u>
45/35	1.52GHz	1.6GHz

Step Two : Broaden the bandwidth

In step two, the chosen antennas (the underlined one) shown in Table 4.1, are shaped into the one as shown in Figure 4.4, which is called the planar binomial antenna [17]. The binomial antenna shows ultra-wideband characteristics. The formula of the binomial curve is shown below [17].

$$f_1(x) = G + (L_{b1} - G) \left(\frac{x}{W_{b1}/2} \right)^4, \quad -\frac{W_{b1}}{2} \leq x \leq \frac{W_{b1}}{2} \quad (4.2)$$

Here, W_{b1} and L_{b1} are the width and length of the binomial patch, respectively, as shown in Figure.4.4. $W = 50$ mm, $L = 45$ mm and $G = 1.6$ mm are fixed for simplification. The wanted bandwidth will be achieved by properly tuning W_{b1} and L_{b1} . From the computed return loss versus frequency as shown in Figure 4.5, it is found that the bandwidth is increased with W_{b1} . From the computed covering frequency band using HFSS listed in Table 4.2 (Up to 4GHz) for different sizes of W_{b1} and L_{b1} , it is found that the operational frequency range is increased with W_{b1} . The low bound of the operational frequency range becomes smaller when L_{b1} increases. By comparing between Figure 4.3 and Figure 4.5, it is found that a binomial curve structure provides with a wider bandwidth than a simple rectangular one.

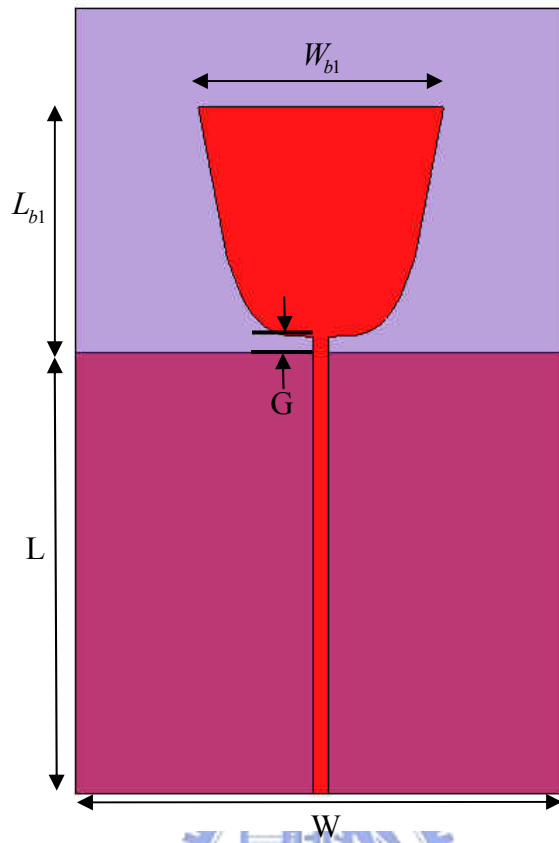


Figure 4.4 The geometry of the planar binomial antenna.

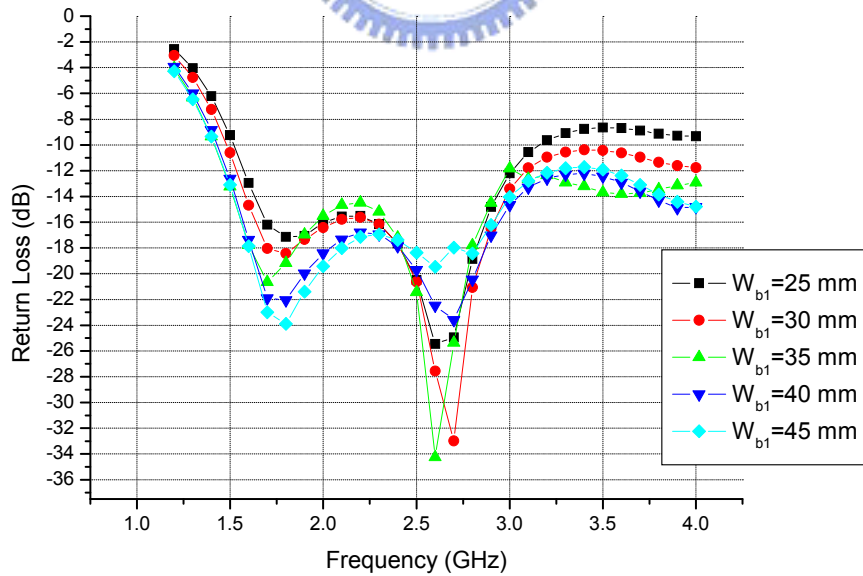


Figure 4.5 The computed return loss versus frequency of the planar binomial antennas with $L_{b1} = 25$ mm .

Table 4.2 Computed bandwidths of the planar binomial antennas.

W_{b1}/L_{b1} (mm/mm)	Operational Frequency Range (GHz)	Bandwidth
25/25	1.6-3.1	1.5 GHz
25/30	1.4-2.9	1.5 GHz
30/25	1.5-4	2.5 GHz
30/30	1.4-4	2.6 GHz
35/25	1.5-4	2.5 GHz
35/30	1.4-4	2.6 GHz
40/25	1.5-4	2.5 GHz
40/30	1.4-4	2.6 GHz
45/25	1.5-4	2.5 GHz
45/30	1.4-4	2.6 GHz

Step Three : Shaping the antenna

In step three, a planar binomial antenna is shaped into the one as shown in Figure 4.6, which is called the planar hybrid-binomial antenna. Current mainly flow in edges of an antenna. Frequency response is changed severely by modifying a shape of edges. Therefore, some edges of the selected planar binomial antenna are selected to cut off. Another binomial formula is selected to cut the end edge of the selected planar binomial antenna in order to sustain the broadband characteristic. The formula is shown below [17]

$$f_2(x) = L_{b2} \times \left(\frac{x}{W_{b2}/2}\right)^4, \quad -\frac{W_{b2}}{2} \leq x \leq \frac{W_{b2}}{2} \quad (4.3)$$

Here, W_{b2} and L_{b2} are the width and length of the binomial cutting area, respectively, as shown in Figure.4.6. $W = 50$ mm and $L = 45$ mm are fixed in this step. $G = 1.6$ mm and $W_{b2} = 25$ mm are fixed for simplification. The wanted bandwidth will be achieved by properly tuning L_{b2} . From the computed return loss versus frequency shown in Figure 4.7, it is found that the bandwidth is decreased with larger L_{b2} . As L_{b2} is varied from 5 to 20 mm, the lower bound of the covering frequency band will shift to a higher value. The components of high frequencies will also cut off. Although a stop frequency band is created in high frequencies, the lower bound of the covering frequency band shift to a higher value. This is not my desired result. So we make a second adjustment.

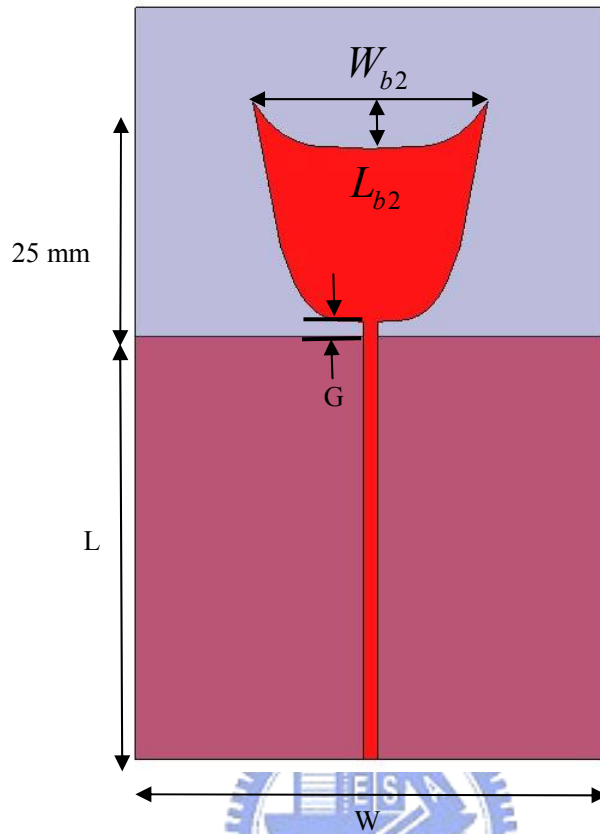


Figure 4.6 The geometry of the planar hybrid-binomial antenna.

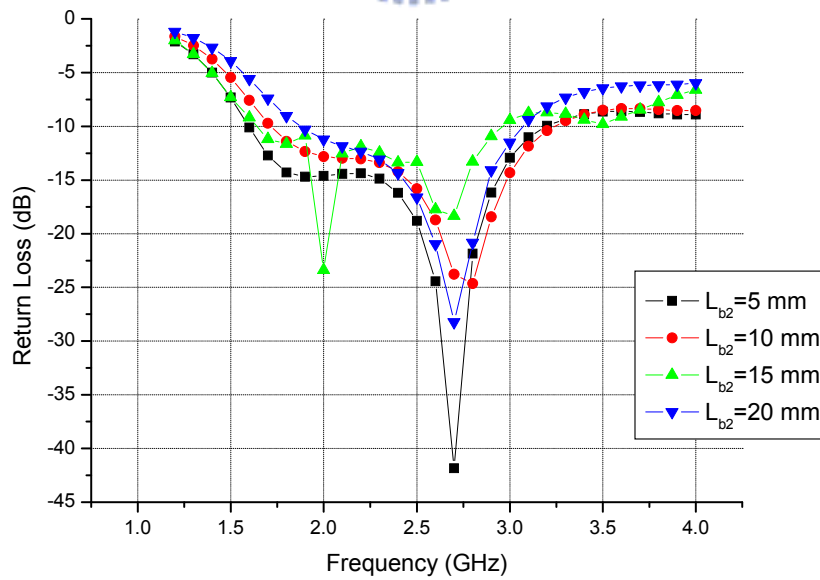


Figure 4.7 The computed return loss versus frequency of the first adjustment,

$$W_{b2} = 25 \text{ mm} .$$

In the second adjustment, we would like to cut off frequency response higher than 2.9 GHz by cutting some parts of a planar binomial antenna and also compensate lower frequency response of the one. The geometry of the modified antenna is shown in Figure 4.8 which is called the planar eagle-shaped antenna. Here, W_c and L_c are the width and length of the cutting area, respectively, as shown in Figure.4.8. $G = 1.6$ mm are fixed for simplification. The wanted bandwidth will be achieved by properly tuning W_c and L_c . From the computed return loss versus frequency shown in Figure 4.9, it is found that the bandwidth is decreased with larger L_c . The resonant frequency will also shift to a lower value with larger W_c . From Figure 4.9, we find that there are two purposes by tuning W_c and L_c . One is to compensate the components of lower frequencies; another is to cut off the components of higher frequencies. The computed current distribution of the unmodified antenna in $f = 1.575$ GHz is shown in Figure 4.10. From Figure4.10, it is found that the current mainly flows along edges of the antenna and the strength of the current magnitude is stronger near the feed point. The computed current distribution of the modified antenna in $f = 1575$ MHz is shown in Figure 4.11. From Figure 4.11, it is found that the current flows along the cutting area. The miniaturization is achieved due to increasing resonant length formed by the cutting area.

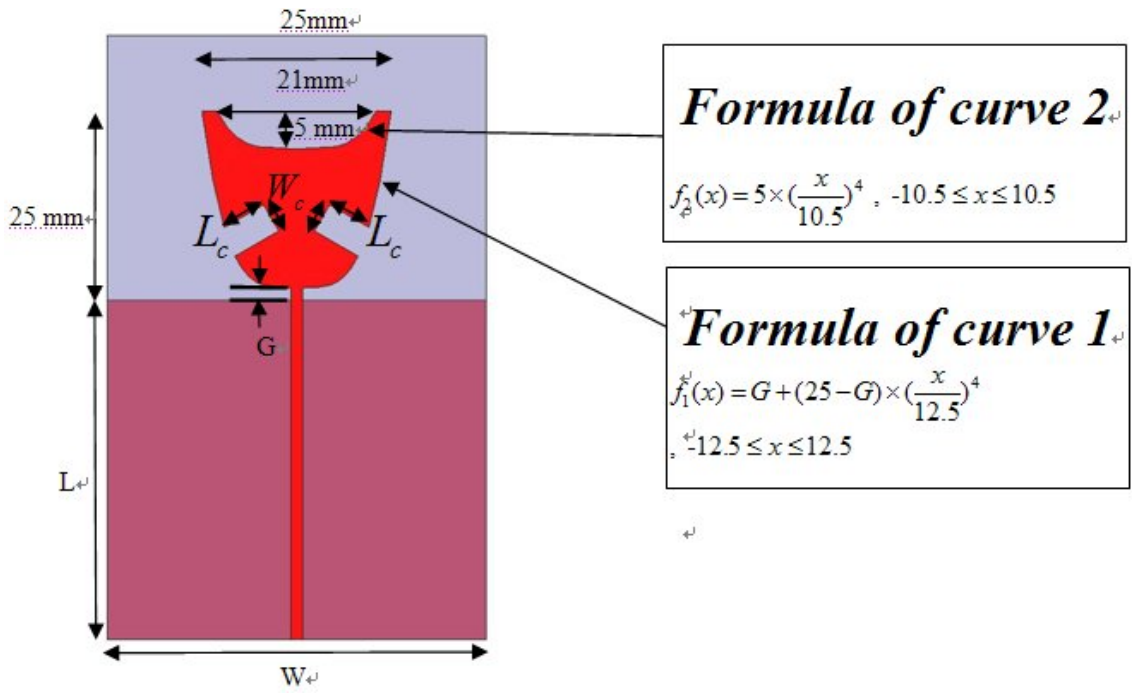
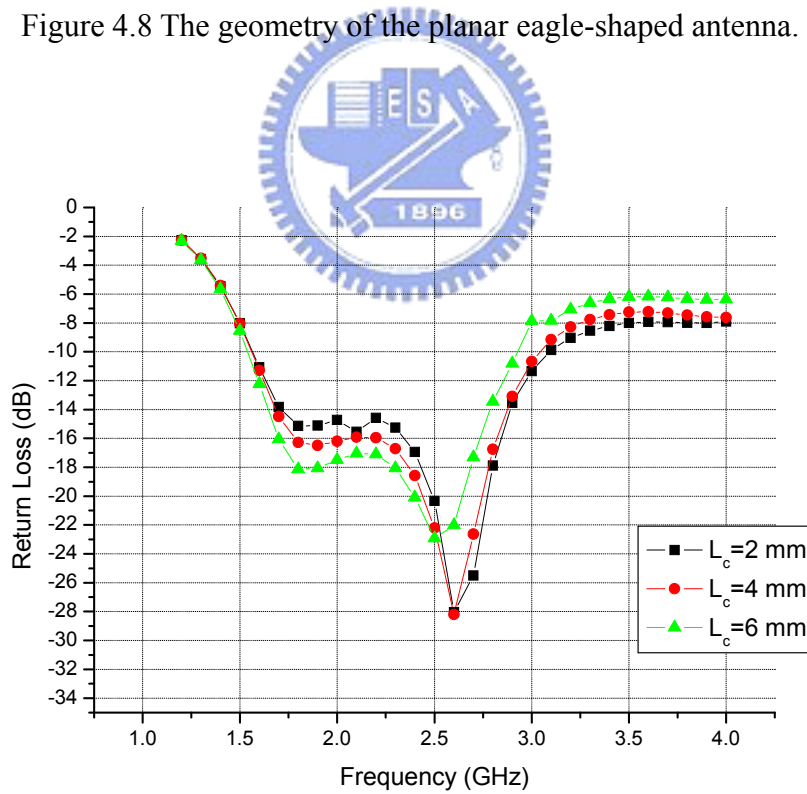
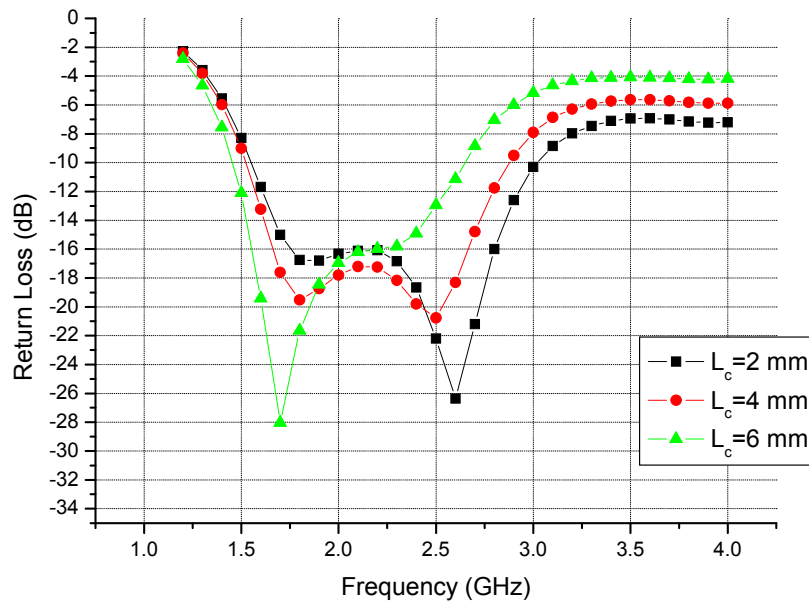


Figure 4.8 The geometry of the planar eagle-shaped antenna.



(a) $W_c = 2 \text{ mm}$



(b) $W_c = 6$ mm

Figure 4.9 The computed return loss versus frequency of the second adjustment

(a) $W_c = 2$ mm (b) $W_c = 6$ mm.

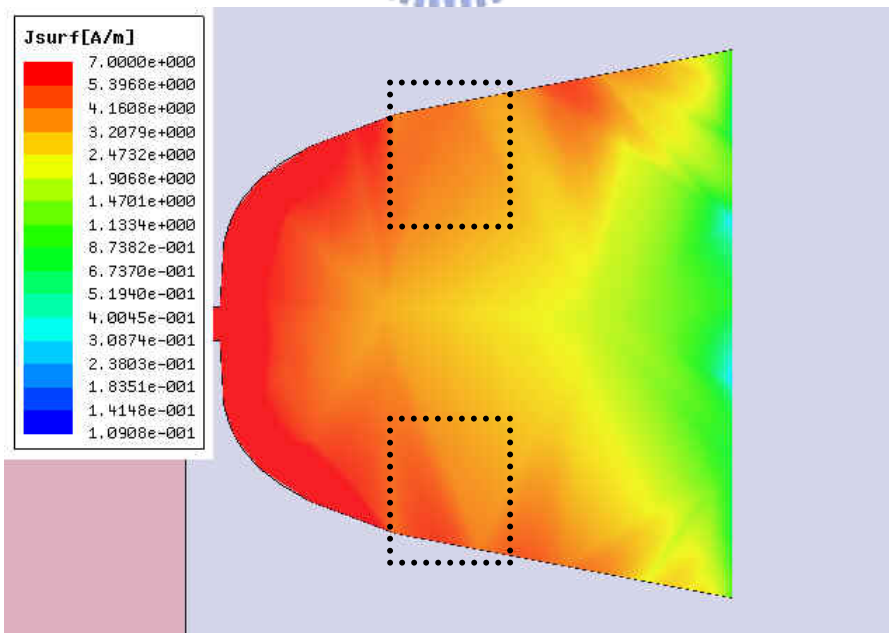


Figure 4.10 The computed current distribution of the unmodified antenna;

$f = 1.575$ GHz, phase=320 degrees.

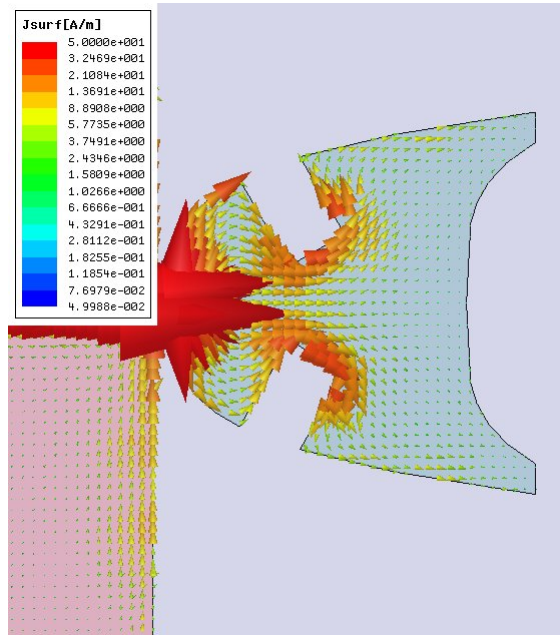


Figure 4.11 The computed current distribution of the modified antenna;
 $f=1.575\text{GHz}$, phase=320 degree.

G is a gap between the ground plane and the antenna as shown in Figure.4.9. In the following discussion, the influence on frequency response will be studied by properly tuning G . $W_c = 4\text{mm}$ and $L_c = 6\text{mm}$ are fixed in this discussion. From the computed return loss versus frequency shown in Figure 4.12, it is found that the resonant frequency will shift to a lower value with larger G . It is simply because that there is a coupling effect between the ground plane and the antenna. The coupling effect is created by two currents flowing on the ground plane and the antenna.

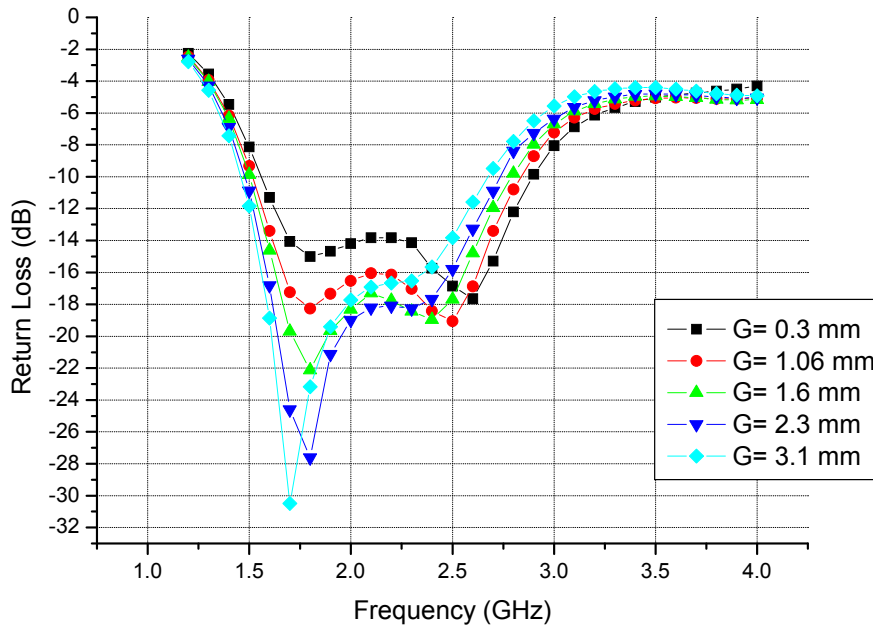


Figure 4.12 The computed return loss versus frequency of the planar eagle-shaped antenna by varying G .

4.2 Comparison of the Computed and Measured Results

After some numerical computations, size of the proposed antenna has been fine tuned and determined as shown in Figure 4.13. The proposed antenna was fabricated using FR4 substrate material. The radiation element is copper. A photograph of the proposed antenna is shown in Figure 4.14. Agilent 8719ET is used for measuring the return loss of the proposed antenna. In Figure 4.15, it is found that the computed and measured return losses versus frequency are close. The computed operating frequency range is 1.49 GHz to 2.78 GHz and the measured operating frequency range is 1.54 GHz to 2.73 GHz. The computed and measured bandwidths are 1.29 GHz and 1.19 GHz, respectively.

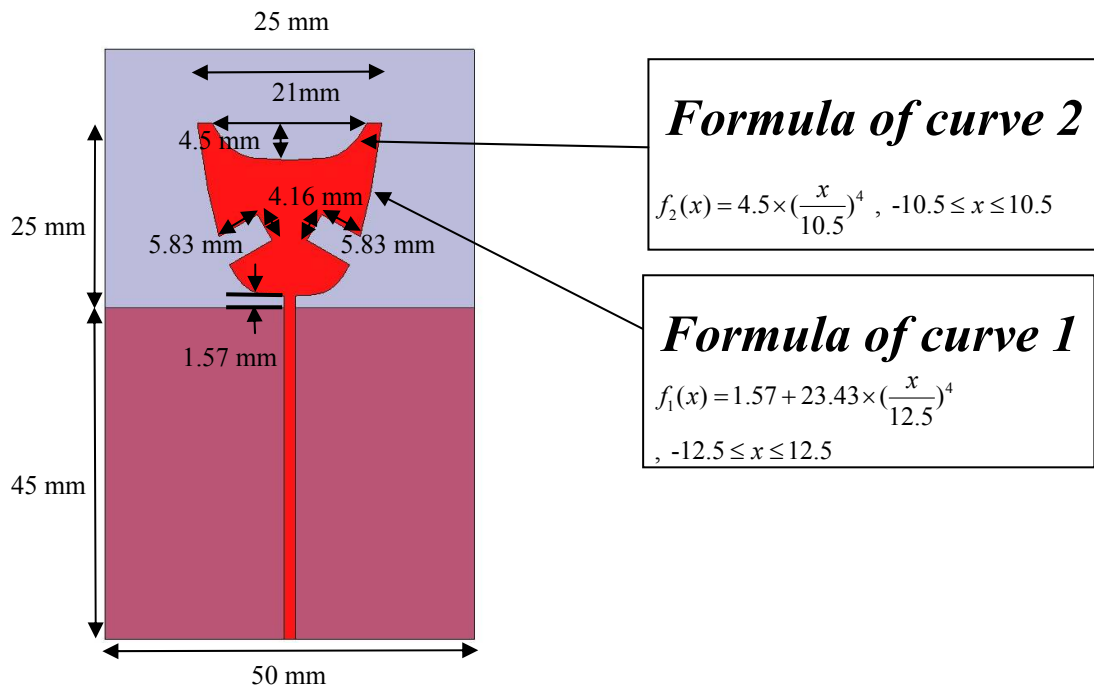


Figure 4.13 The geometry of the proposed antenna.



Figure 4.14 The photograph of the proposed antenna.

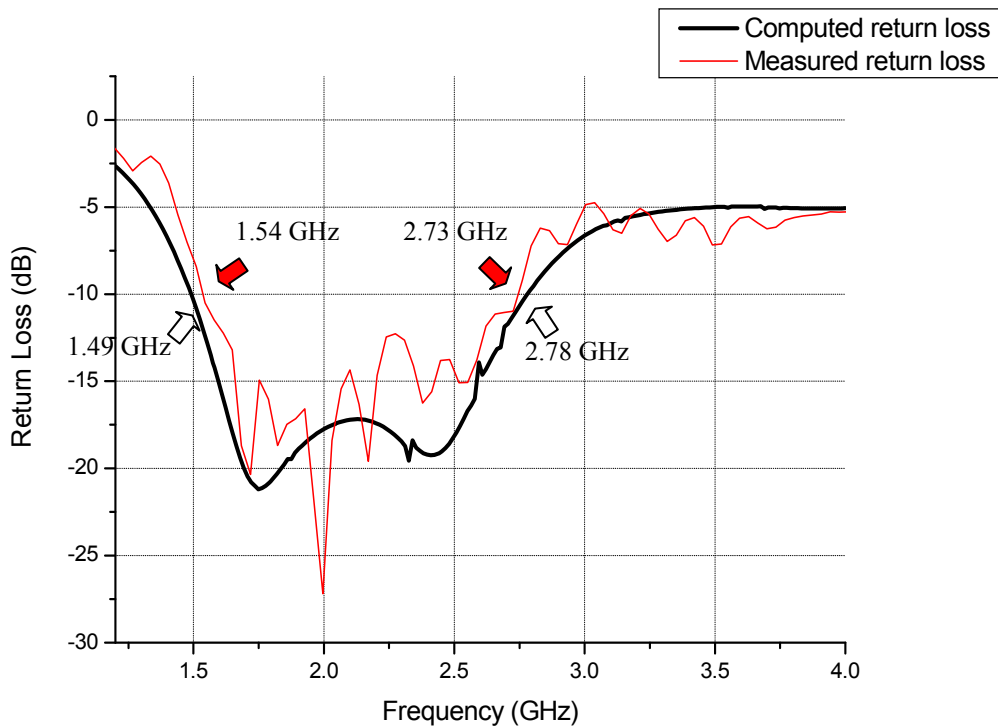


Figure 4.15 The computed and measured return losses versus frequency of the proposed antenna.



The far-field radiation pattern of the antenna is measured in an anechoic chamber. The computed radiation patterns are shown in Figures 4.16, 4.17,....., and Figure 4.21 for 1575 MHz, 1795 MHz, 1920 MHz, 2045 MHz, 2442 MHz and 2595 MHz, respectively. The measured radiation patterns are shown in Figures 4.22, 4.23,....., and Figure 4.27 for 1575 MHz, 1795 MHz, 1920 MHz, 2045 MHz, 2442 MHz and 2595 MHz, respectively. From measured radiation patterns, it is found that the radiation strength is the smallest at the feed point. The radiation patterns are nearly omni-directional. The radiation gains are between 2.25 and 3.74 dBi. Measured radiation patterns are asymmetric that maybe due to the effects of FR4 heterogeneity and/or the measurement system/environment.

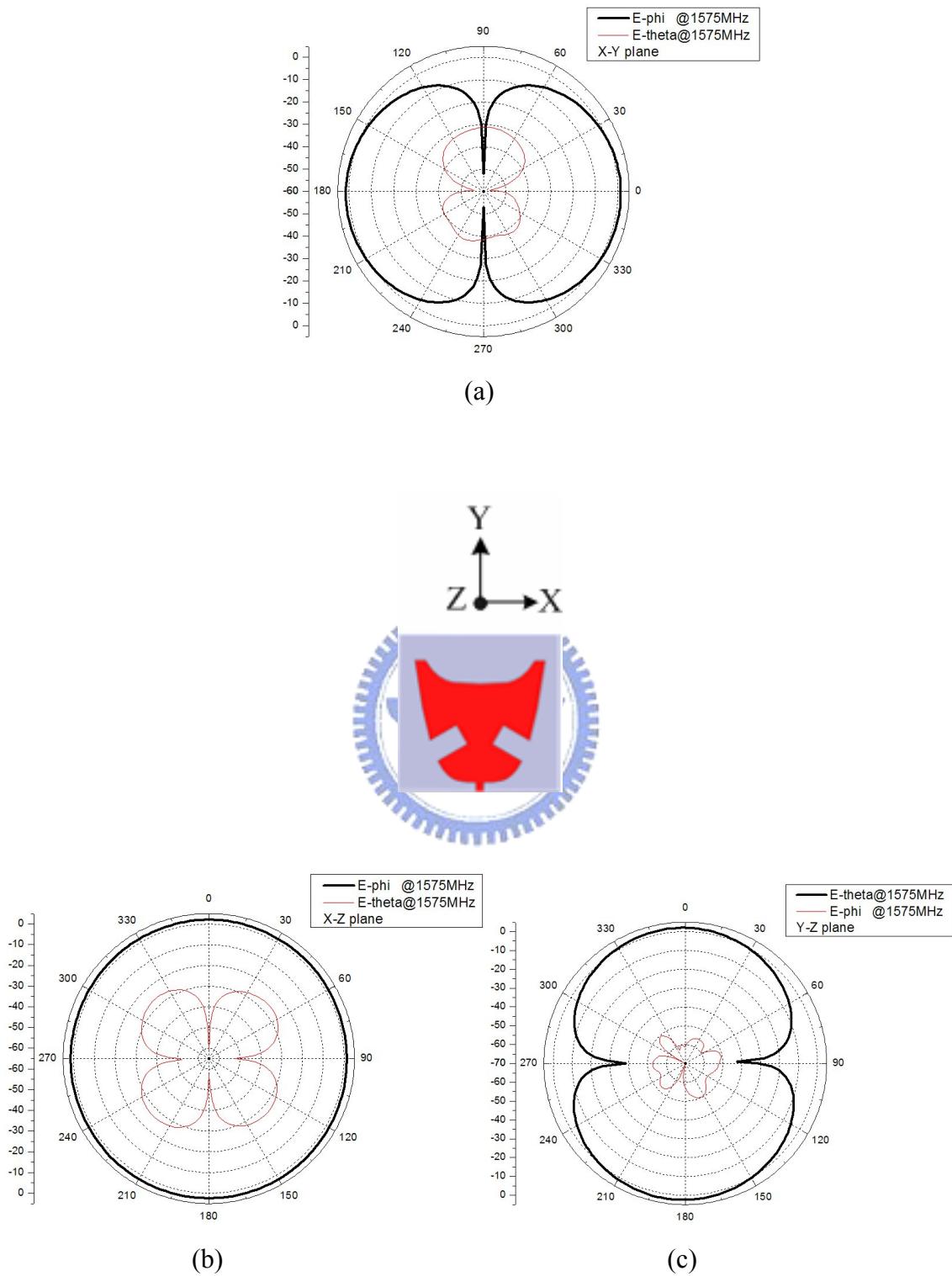


Figure 4.16 The computed radiation patterns of the proposed antenna (1575 MHz)

(a)X-Y plane (b) X-Z plane (c) Y-Z plane.

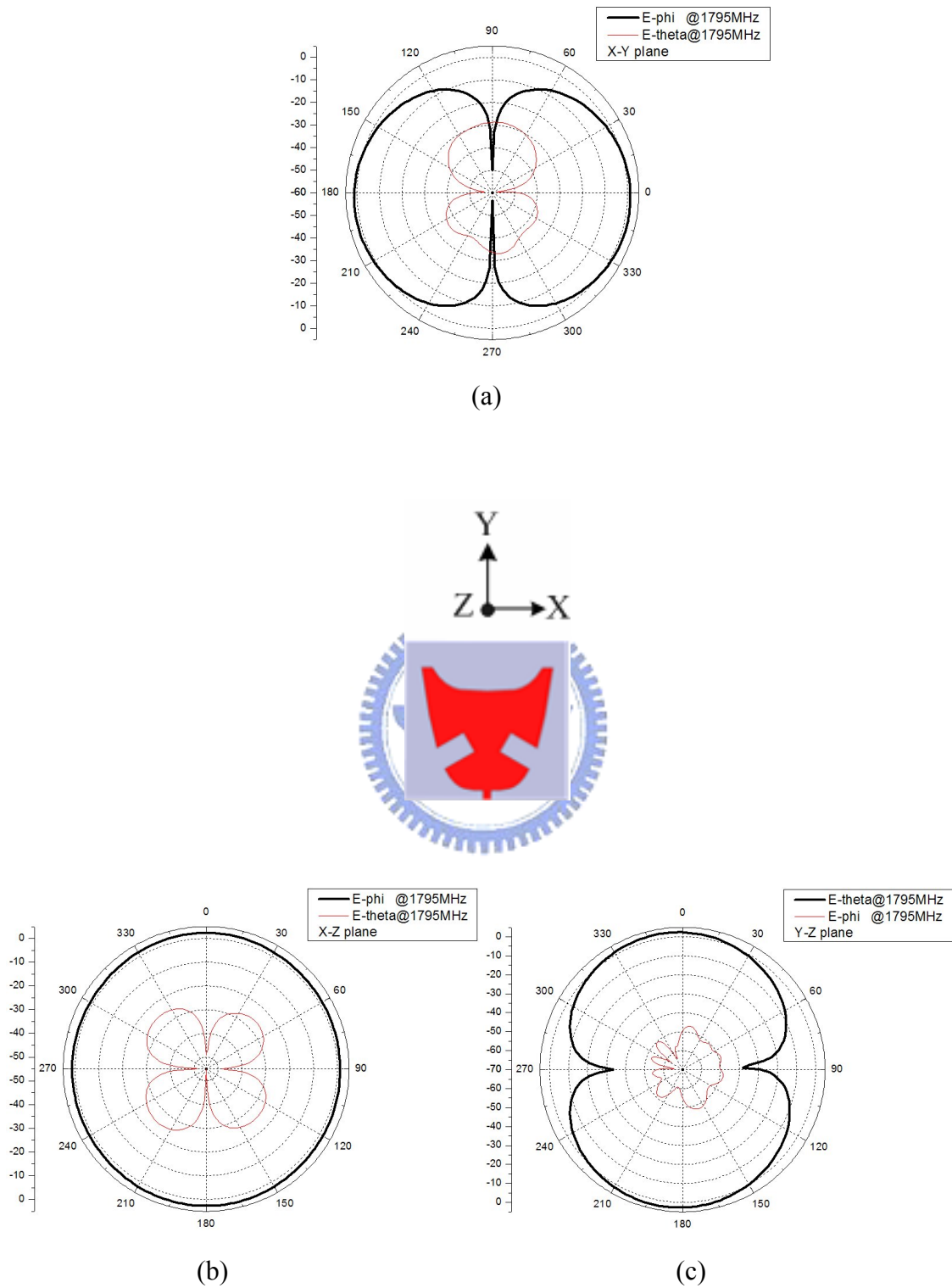


Figure 4.17 The computed radiation patterns of the proposed antenna (1795 MHz)

(a) X-Y plane (b) X-Z plane (c) Y-Z plane.

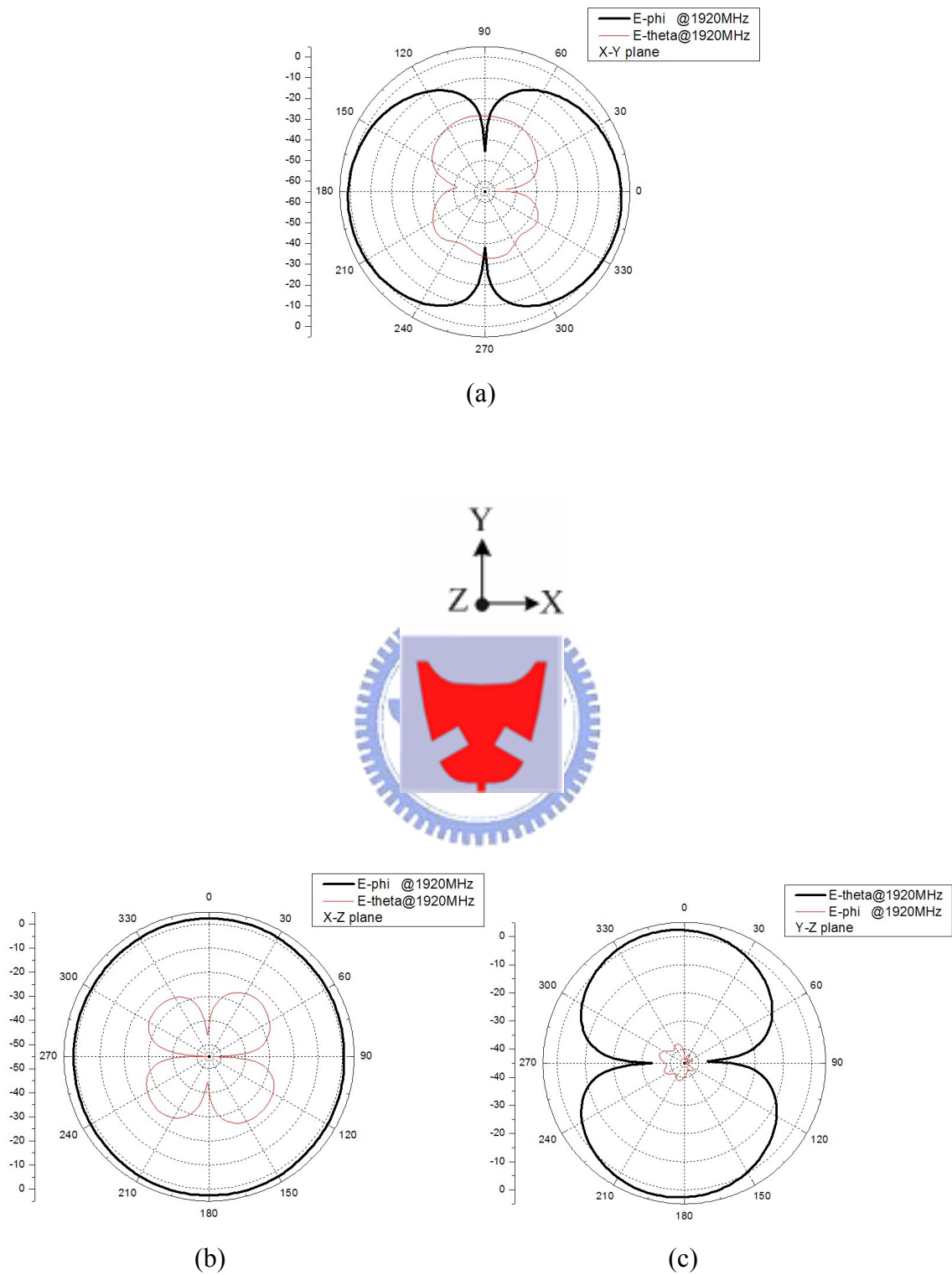


Figure 4.18 The computed radiation patterns of the proposed antenna (1920 MHz)

(a) X-Y plane (b) X-Z plane (c) Y-Z plane.

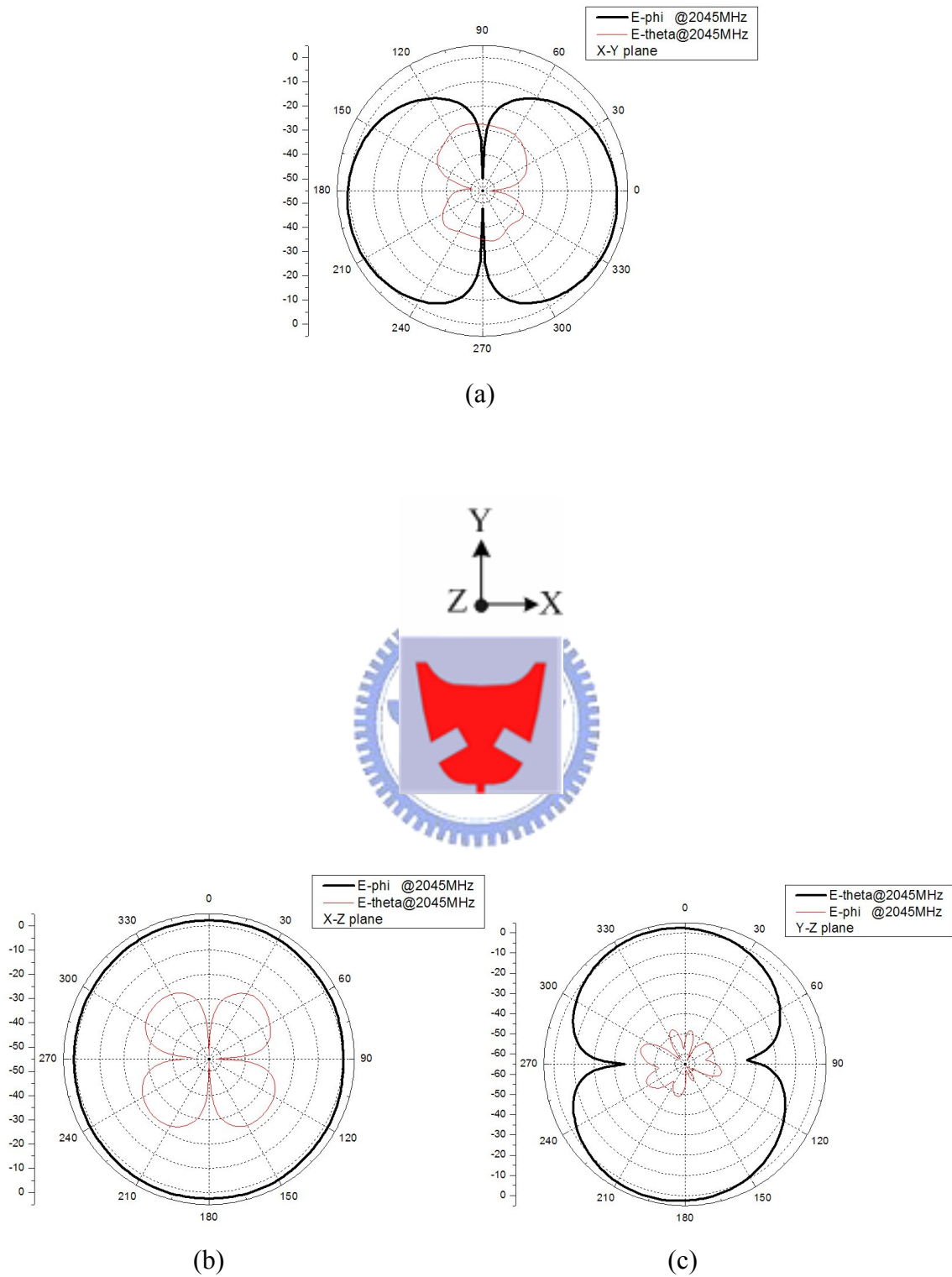


Figure 4.19 The computed radiation patterns of the proposed antenna (2045 MHz)

(a) X-Y plane (b) X-Z plane (c) Y-Z plane.

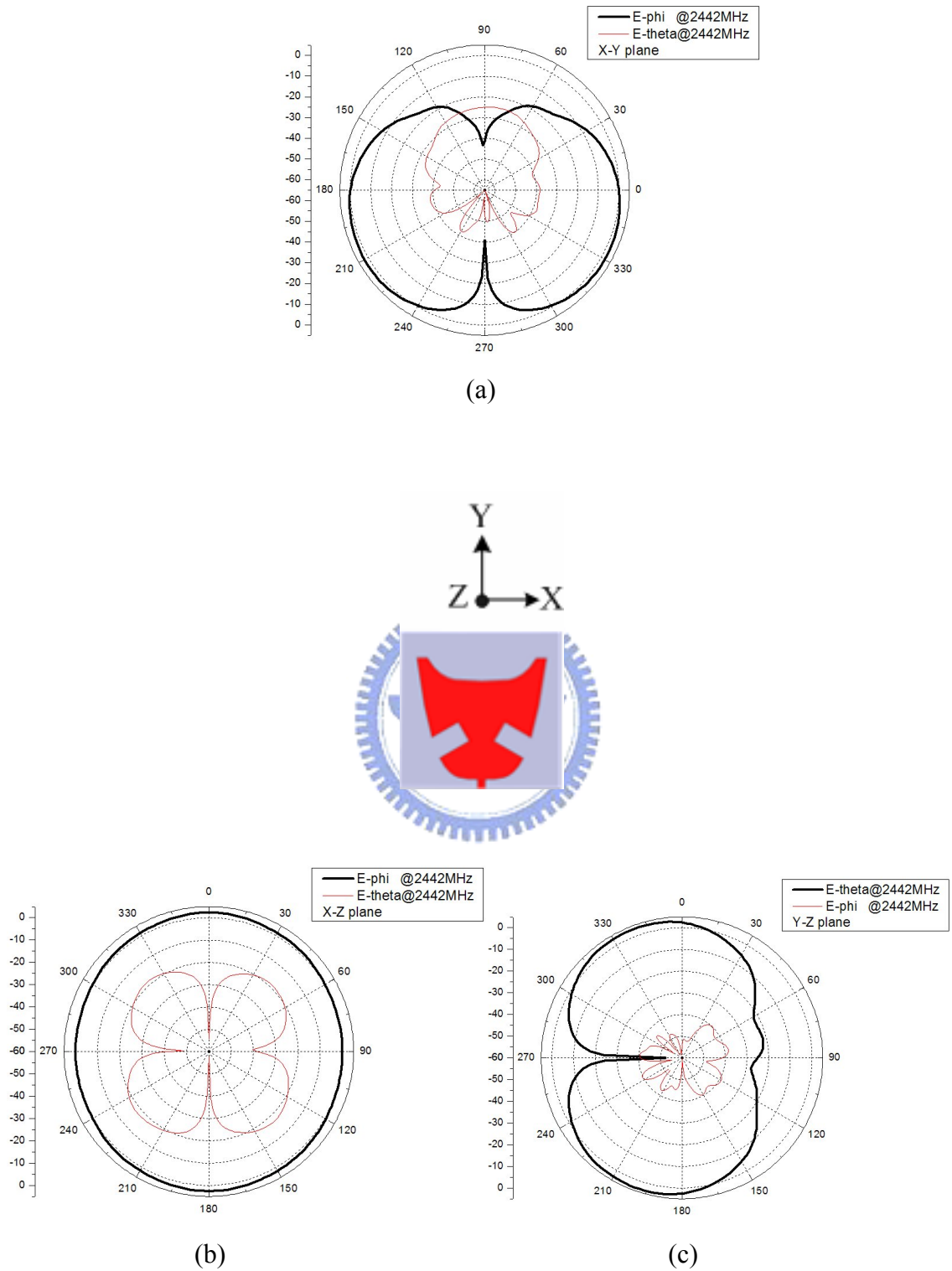


Figure 4.20 The computed radiation patterns of the proposed antenna (2442 MHz)

(a) X-Y plane (b) X-Z plane (c) Y-Z plane.

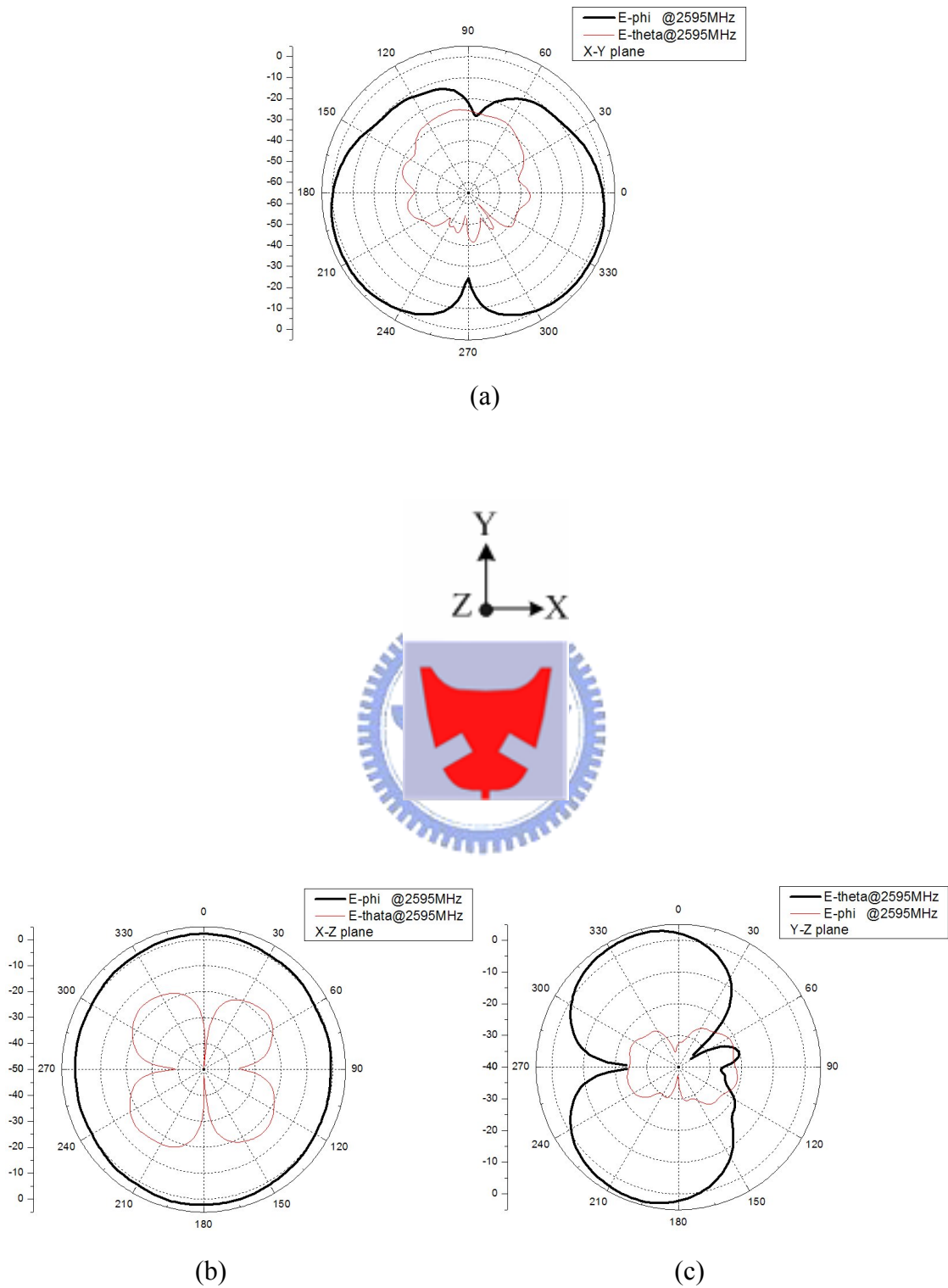


Figure 4.21 The computed radiation patterns of the proposed antenna (2595 MHz)

(a) X-Y plane (b) X-Z plane (c) Y-Z plane.

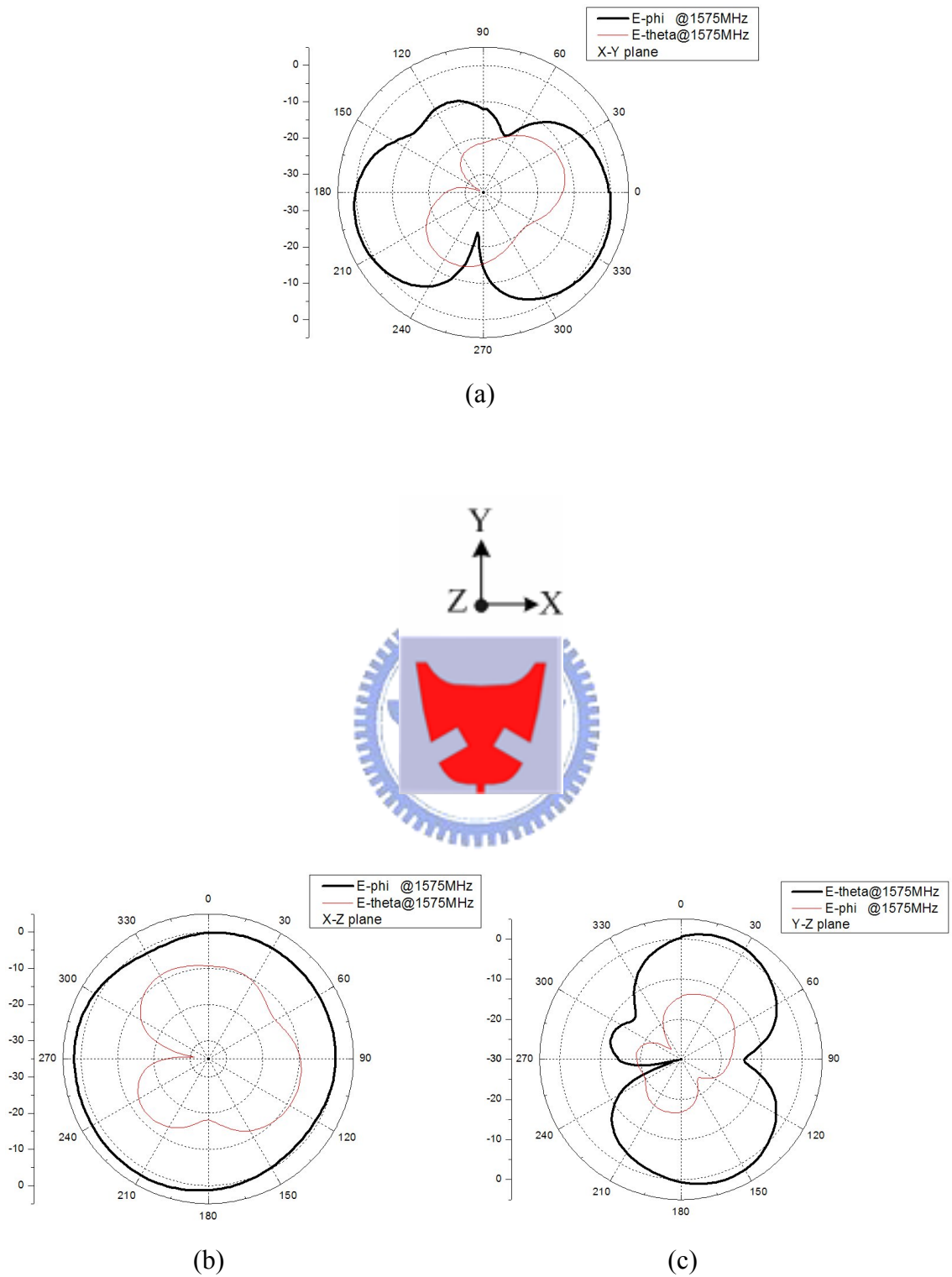
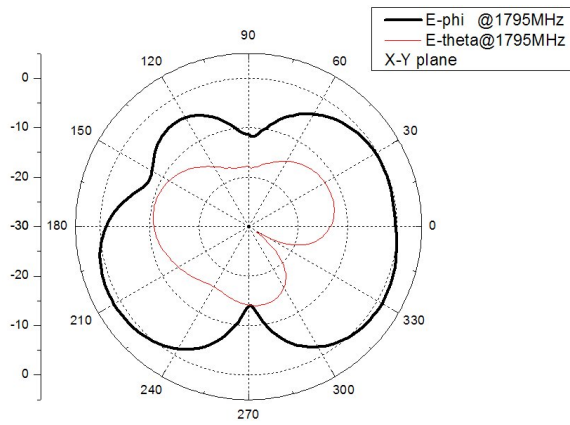
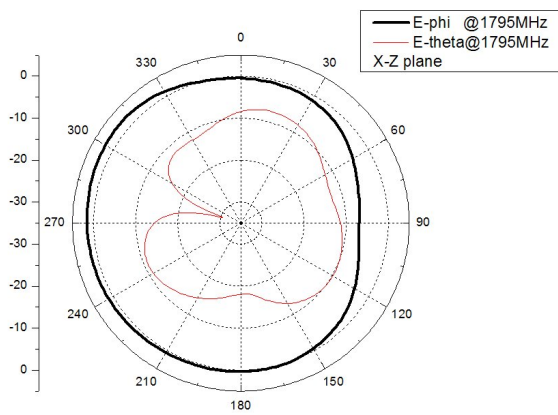
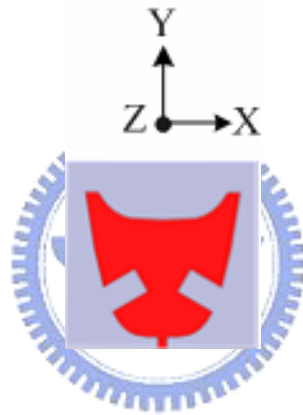


Figure 4.22 The measured radiation patterns of the proposed antenna (1575 MHz)

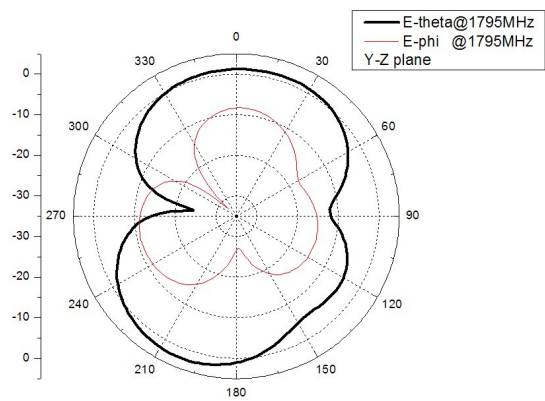
(a)X-Y plane (b) X-Z plane (c) Y-Z plane.



(a)



(b)



(c)

Figure 4.23 The measured radiation patterns of the proposed antenna (1795 MHz)

(a) X-Y plane (b) X-Z plane (c) Y-Z plane.

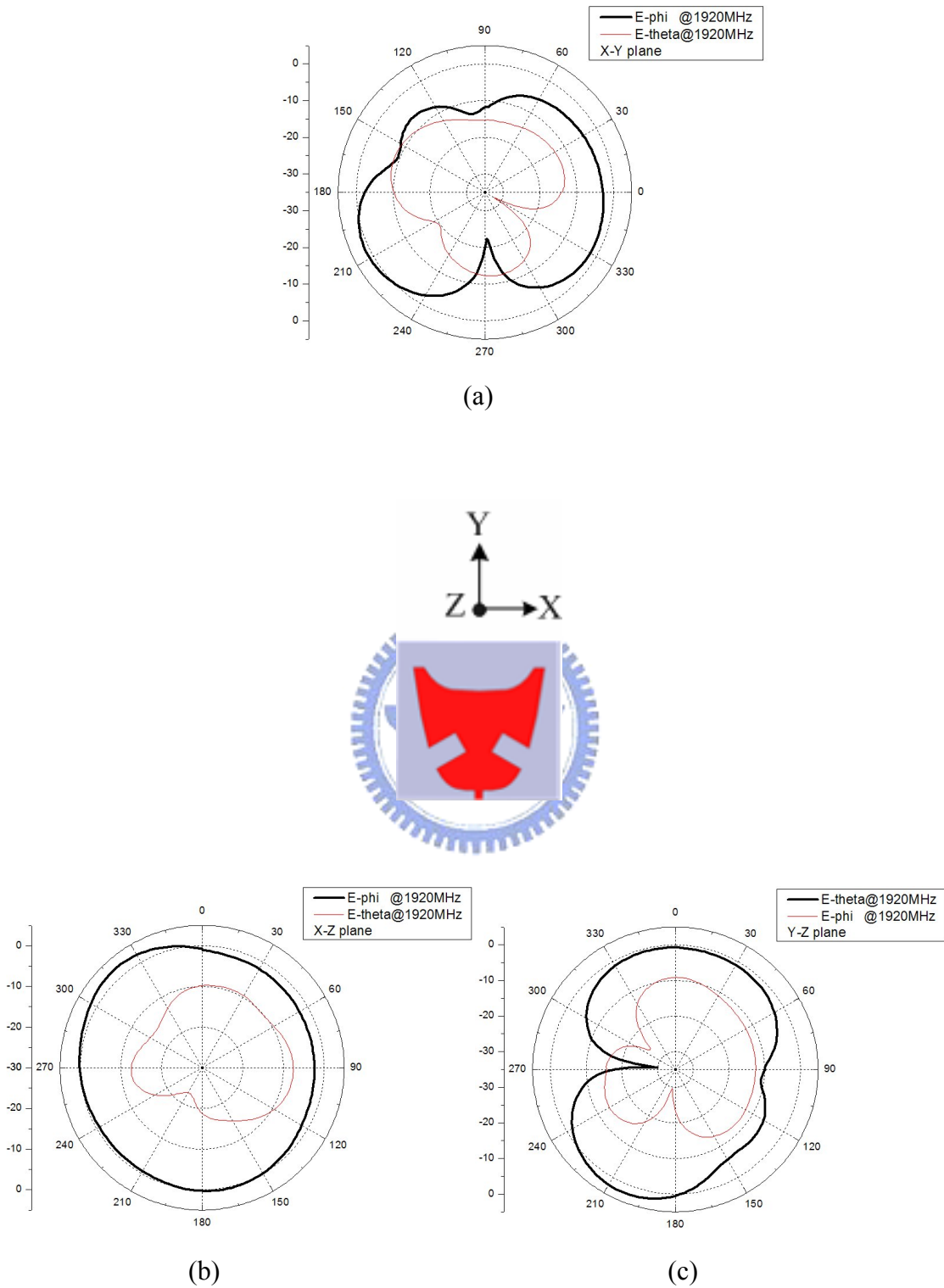


Figure 4.24 The measured radiation patterns of the proposed antenna (1920 MHz)

(a) X-Y plane (b) X-Z plane (c) Y-Z plane.

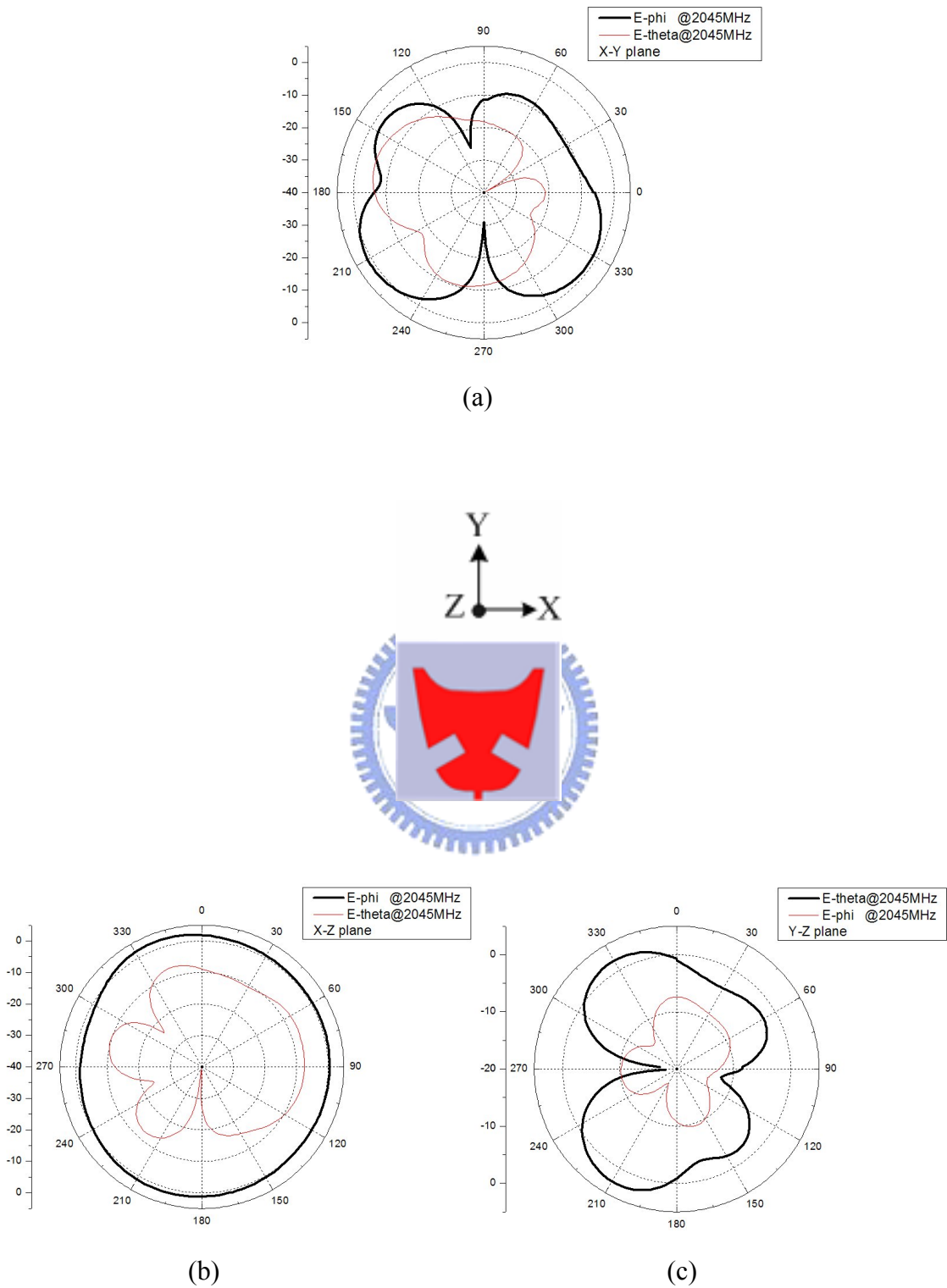


Figure 4.25 The measured radiation patterns of the proposed antenna (2045 MHz)

(a) X-Y plane (b) X-Z plane (c) Y-Z plane.

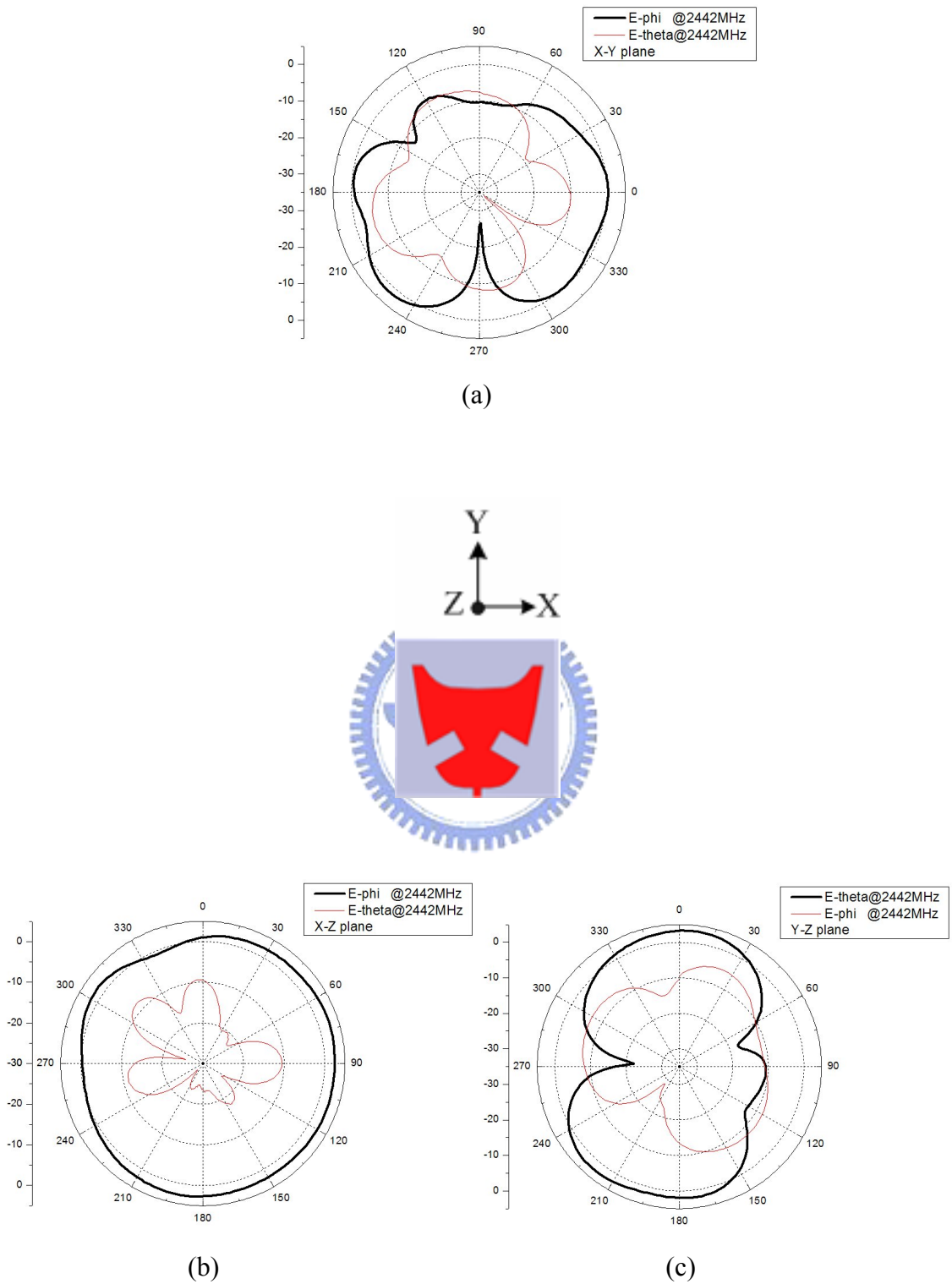


Figure 4.26 The measured radiation patterns of the proposed antenna (2442 MHz)

(a) X-Y plane (b) X-Z plane (c) Y-Z plane.

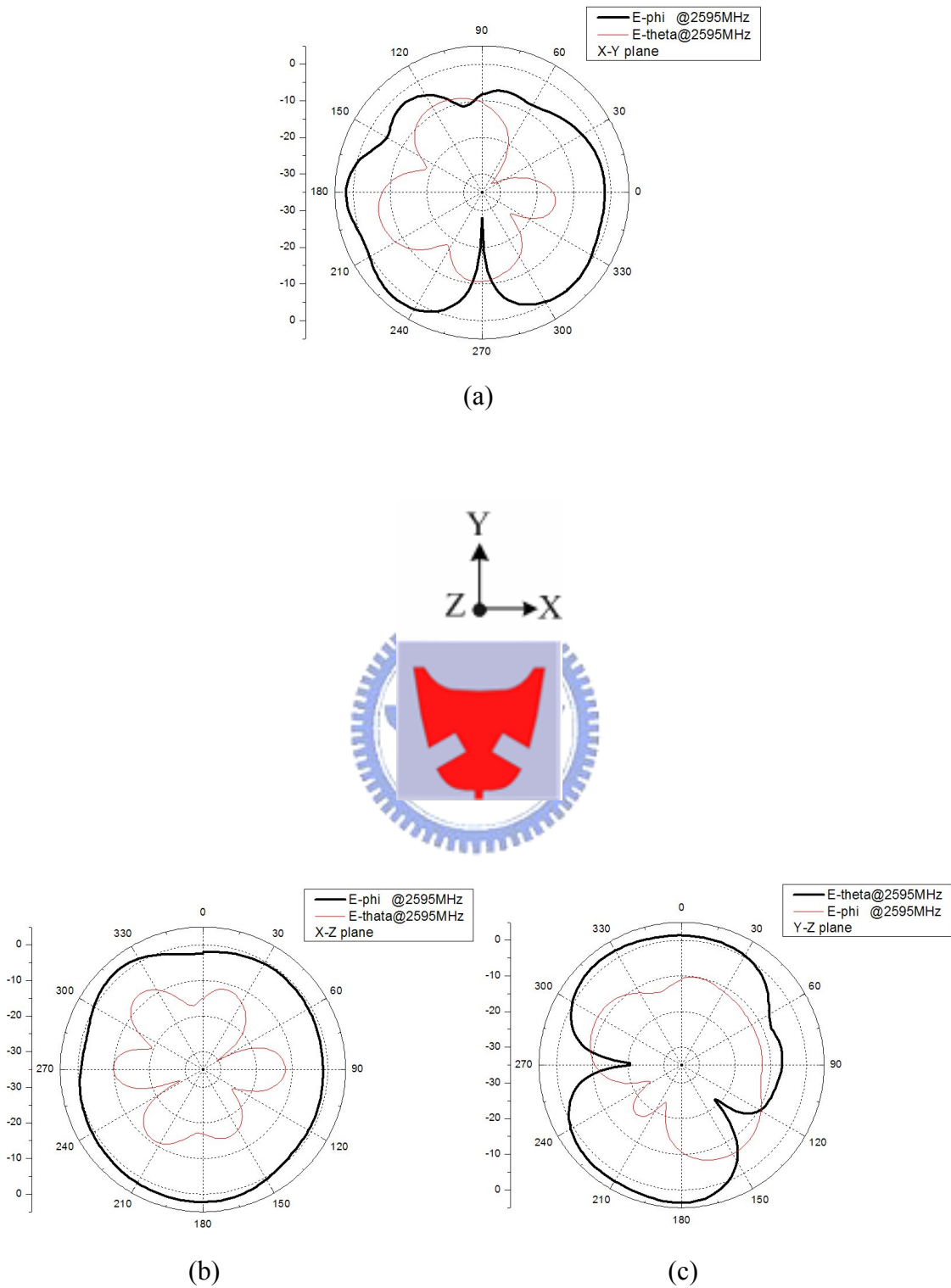


Figure 4.27 The measured radiation patterns of the proposed antenna (2595 MHz)

(a) X-Y plane (b) X-Z plane (c) Y-Z plane.

The computed and measured peak gains of six frequencies are listed in Table 4.3. The computed radiation efficiencies of six frequencies are also listed in Table 4.3. It is found that the computed and measured peak gains of six frequencies are approximate. The inaccuracy between the computed and measured results maybe causes by the effects of measurement system/environment. The measured gains are reasonable and the computed radiation efficiencies are high. The comparison to other published works is listed in Table 4.4. It is found that the proposed antenna occupies a compact volume of $25 \times 25 \times 0.8 \text{ mm}^3$, which is smaller than other designs of the volumes: 600 mm^3 , 1135 mm^3 , 1181 mm^3 or 1598 mm^3 . From above results, it is found that the proposed antenna is suitable for applications of mobile phones.

Table4.3 The computed and measured peak gains, the computed radiation efficiencies of six frequencies.

Frequency (MHz)	1575	1795	1920	2045	2442	2595
Computed peak gain (dBi)	2.44	2.79	2.85	2.96	3.58	3.84
Measured peak gain (dBi)	2.25	2.53	2.54	2.92	3.7	3.74
Radiation efficiencies (%)	94.4	94.6	94.3	94	93.7	92.8

Table4.4 Comparison to other published works.

Paper	Size (mm^3)	Operating frequency range	Antenna gain
[1]	50x30x0.4(600)	About 1000-2400MHz (1400 MHz)	2-4.5 dBi
[2]	33x21.5x1.6(1135)	1460-2680 MHz (1220 MHz)	0-4.1 dBi
[4]	20x17x4.7(1598)	1620-2360 MHz (740 MHz)	2.3-3.1 dBi
[5]	27x12.5x3.5(1181)	1710-2510 MHz (800 MHz)	1.71-3.47 dBi
Proposed antenna	25x25x0.8(500)	1540-2730 MHz (1190 MHz)	2.25-3.74 dBi

Chapter 5 Conclusion

In this thesis, a special eagle-shaped antenna is proposed. The binomial structure plays an important role in achieving broadband characteristic. The miniaturization is achieved by increasing resonant length with cutting edges. The experimental results have validated the simulation ones. The operating band of the proposed antenna is 1.54 GHz to 2.73 GHz and the proposed antenna is suitable for GPS, GSM 1800, PCS, 3G, WLAN, and WiMAX applications. The antenna occupies a compact volume of $25 \times 25 \times 0.8 \text{ mm}^3$ and is small enough to be placed on the internal area of practical mobile handsets. The simulated and measured results show that the proposed antenna offers the broadband bandwidth, the radiated efficiencies of more than 92 %, and has almost omni-directional radiated patterns over the entire operating band.

Reference

-
- [1] Zhengwei Du, Ke Gong, and Jeffrey Shiang Fu, “A Novel Compact Wide-Band Planar Antenna for Mobile Handsets,” *IEEE Transactions on Antennas and Propagation*, vol. 54, no. 2, Feb. 2006.
- [2] Tayeb A. Denidni, Hyeonjin Lee, Yeongseog Lim, and Qinjiang Rao, “Wide-Band High-Efficiency Printed Loop Antenna Design for Wireless Communication Systems,” *IEEE Transactions on Vehicular Technology*, vol. 54, no. 3, May 2005.
- [3] K.-L. Wong, G.-Y. Lee, and T.-W. Chiou, “A Low-Profile Planar Monopole Antenna for Multi-band Operation of Mobile Handsets,” *IEEE Transactions on Antennas and Propagation*, vol. 51, pp. 121–125, Jan. 2003.
- [4] Yong-Sun Shin, Seong-Ook Park, and Manjai Lee, “A Broadband Interior Antenna of Planar Monopole Type in Handsets,” *IEEE Antennas and Wireless Propagation Letters*, vol. 4, 2005.
- [5] Dong-Uk Sim and Seong-Ook Park, “A Triple-Band Internal Antenna: Design and Performance in Presence of the Handset Case, Battery, and Human Head,” *IEEE*

- Transactions on Electromagnetic Compatibility*, vol. 47, no. 3, Aug. 2005.
- [6] S.-H. Yeh, K.-L. Wong, T.-W. Chiou, and S.-T. Fang, "Dual-Band Planar Inverted F Antenna for GSM/DCS Mobile Phones," *IEEE Transactions on Antennas and Propagation*, vol. 51, no. 5, pp. 1124–1126, May 2003.
- [7] C. W. Chiu and F. L. Lin, "Compact Dual-Band PIFA with Multi-Resonators," *Electronics Letters*, vol. 38, pp. 538–540, 2002.
- [8] D. Manteuffel, A. Bahr, D. Heberling, and I. Wolff, "Design Considerations for Integrated Mobile Phone Antennas," in *Proc. 11th Int. Conference Antennas and Propagation*, vol. 1, pp. 252–256, 2001.
- [9] Y. J. Wang, C. K. Lee, W. J. Koh, and Y. B. Gan, "Design of Small and Broad-Band Internal Antennas for IMT-2000 Mobile Handsets," *IEEE Transactions on Microwave Theory and Techniques*, vol. 49, pp. 1398–1403, Aug. 2001.
- [10] Constantine A. Balanis, *Antenna Theory: Analysis and Design*, 3rd ed., John Wiley & Sons, Inc., 2005.
- [11] Kin-Lu Wong, *Compact and Broadband Microstrip Antennas*, John Wiley & Sons, Inc., 2002.
- [12] Thomas S. Laverghetta, "Microwaves and Wireless simplified, Second Edition," ARTECH HOUSE, Inc., 2005.
- [13] Kin-Lu Wong, *Planar Antennas For Wireless Communications*, John Wiley & Sons, Inc., 2003.
- [14] Kyeong-Sik Min, Tran Viet Hong, and Duk-Woo Kim, "A Design of a Meander Line Antenna using Magneto-Dielectric Material for RFID System," *APMC2005 Proceedings*.
- [15] 湯譯增, 劉耿宏, 陳文立, 林丁丙, 洪瑞鴻, "超寬頻天線小型化之設計與分析," 全國電信研討會, 2006.
- [16] 羅文信, "新型縮小化超寬頻印刷式天線設計," 國立交通大學碩士論文, 2004.

- [17] Warren L. Stutzman and Gary A. Thiele, *Antenna Theory and Design*, 2nd ed., John Wiley & Sons, Inc., 1998.
- [18] David M. Pozar, *Microwave Engineering*, 3rd ed., John Wiley & Sons, Inc., 2005.
- [19] K. L. Wong, C. L. Tang, and H. T. Chen, “A Compact Meandered Circular Microstrip Antenna with A Shorting Pin,” *Microwave and Optical Technology Letters* 15, 147–149, June 20, 1997.
- [20] Dr. Otman El Mrabet, “High Frequency Structure Simulator (HFSS)Tutorial, ”*IETR, UMR CNRS 6164, INSA, 20 avenue Butte des Coësmes 35043 Rennes, FRANCE*, 2006.
- [21] W. Choi, S. Kwon, and B. Lee, “Ceramic Chip Antenna Using Meander Conductor Lines,” *Electronics Letters*, vol. 37, pp. 933–934, Jul. 2001.

